Progress in Biophysics and Molecular Biology xxx (xxxx) xxx

Contents lists available at ScienceDirect

Progress in Biophysics and Molecular Biology

journal homepage: www.elsevier.com/locate/pbiomolbio

Further insights into the molecular complexity of the human sinus node – The role of 'novel' transcription factors and microRNAs

Abimbola J. Aminu [a], Maria Petkova [a], Andrew J. Atkinson [a], Joseph Yanni [a], Alex D. Morris [a], Robert T. Simms [a], Weixuan Chen [a], Zeyuan Yin [a], Marcin Kuniewicz [a, e], Mateusz K. Holda [a, e], Vladislav S. Kuzmin [f], Filip Perde [b], Peter Molenaar [c, d], Halina Dobrzynski [a, e, *]

[a] The Division of Cardiovascular Sciences, University of Manchester, United Kingdom
[b] National Institute of Legal Medicine, Bucharest, Romania
[c] School of Biomedical Sciences, Queensland University of Technology, Brisbane, Australia
[d] Cardiovascular Molecular & Therapeutics Translational Research Group, University of Queensland, The Prince Charles Hospital, Brisbane, Australia
[e] Department of Anatomy, Jagiellonian University Medical College, Krakow, Poland
[f] Department of Human and Animal Physiology, Lomonosov Moscow State University, Moscow, Russia

ARTICLE INFO

Article history:
Received 2 February 2021
Received in revised form
26 April 2021
Accepted 29 April 2021
Available online xxx

Keywords:
Transcription factors
microRNAs
Sinus node dysfunction
Immune cells
Funny channel
Heart rate

ABSTRACT

Research purpose: The sinus node (SN) is the heart's primary pacemaker. Key ion channels (mainly the funny channel, HCN4) and Ca^{2+}-handling proteins in the SN are responsible for its function. Transcription factors (TFs) regulate gene expression through inhibition or activation and microRNAs (miRs) do this through inhibition. There is high expression of macrophages and mast cells within the SN connective tissue. 'Novel'/unexplored TFs and miRs in the regulation of ion channels and immune cells in the SN are not well understood. Using RNAseq and bioinformatics, the expression profile and predicted interaction of key TFs and cell markers with key miRs in the adult human SN vs. right atrial tissue (RA) were determined.

Principal results: 68 and 60 TFs significantly more or less expressed in the SN vs. RA respectively. Among those more expressed were ISL1 and TBX3 (involved in embryonic development of the SN) and 'novel' RUNX1-2, CEBPA, GLI1-2 and SOX2. These TFs were predicted to regulate HCN4 expression in the SN. Markers for different cells: fibroblasts (COL1A1), fat (FABP4), macrophages (CSF1R and CD209), natural killer (GZMA) and mast (TPSAB1) were significantly more expressed in the SN vs. RA. Interestingly, RUNX1-3, CEBPA and GLI1 also regulate expression of these cells. MiR-486-3p inhibits HCN4 and markers involved in immune response.

Major conclusions: In conclusion, RUNX1-2, CSF1R, TPSAB1, COL1A1 and HCN4 are highly expressed in the SN but not miR-486-3p. Their complex interactions can be used to treat SN dysfunction such as bradycardia. Interestingly, another research group recently reported miR-486-3p is upregulated in blood samples from severe COVID-19 patients who suffer from bradycardia.

1. Introduction

The sinus node (SN) is the heart's primary pacemaker because of its unique morphological, molecular and functional properties (Dobrzynski et al., 2013). Anatomical studies show that the human SN is an extended complex crescent-shaped structure that is located at the superior vena cava and right atrium junction, extending along the crista terminalis (Stephenson et al. 2012, 2017; Chandler et al., 2009).

Since the discovery of the SN in 1907 (Keith and Flack 1907), the molecular mechanisms that regulate the pacemaking and conduction function of the SN remain an area of intense exploration. The SN has a unique expression of ion channels, Ca^{2+} handling proteins previously analysed in the human SN by our group (Chandler et al., 2009). These ion channels and Ca^{2+} handling

* Corresponding author. Address: CTF Building, 46 Grafton Street, Manchester, M13 9NT, UK.
E-mail address: halina.dobrzynski@manchester.ac.uk (H. Dobrzynski).

https://doi.org/10.1016/j.pbiomolbio.2021.04.008

proteins are responsible for the membrane voltage and Ca^{2+} clocks - two main mechanisms that are involved in maintaining the SN automaticity which has recently been elegantly summarised by DiFrancesco, D., 2020 in his mini review (DiFrancesco 2020).

An interesting "funny journey" involved in the so-called membrane clock, started with Brown, DiFrancesco and Noble in the late 70's when they discovered the "funny" current (I_f) (Brown et al. 1979). Since then I_f has been expensively studied by DiFrancesco and colleagues (see DiFrancesco D. 2020 for all relevant references) (DiFrancesco 2020). This current is generated by hyperpolarisation-activated cyclic nucleotide-gated channels, activated by cyclic adenosine monophosphate (cAMP), during phase 4 of the SN's action potential. The main isoform of the funny channel, HCN4, is highly expressed in the human SN (Dobrzynski et al., 2013).

Through activation or inhibition of their targets, transcription factors (TFs) regulate the expression of ion channels, Ca^{2+}-handing proteins and other molecules involved in SN function. T-box factors (TBX3, TBX5 and TBX18) and homeodomain factors (SHOX2, ISL1 and NKX2-5) are crucial TFs that are well established to be involved in the development of the SN, heart embryogenesis and are also expressed in adulthood (Petkova et al., 2020; Hoogaars et al., 2007; Christoffels et al., 2010). In the SN, these TFs enhance the expression of genes that are more abundant in the SN (e.g., HCN4) and suppress those that are less expressed in the SN (e.g. cardiac Na^+ channel, SCN5A/Na_v1.5 and main cardiac gap junctional channel, Cx43) (Park and Fishman 2017).

In many tissues including the heart, small non-coding RNA molecules (microRNAs, miRs) regulate the post-transcriptional expression of many protein-coding genes (Thum et al., 2007; Callis and Wang 2008).

We have recently shown that there is complex expression of key miRs involved in pacemaking mechanisms and we confirmed that miR-486-3p regulates HCN4 expression leading to bradycardia when upregulated in the rodent SN (Petkova et al., 2020).

The SN is embedded in an extensive connective tissue as we have previously shown (Chandler et al., 2009; Kharche et al., 2017). Within this connective tissue, there are many elastic fibres and non-cardiac cell types such as fibroblasts, macrophages, mast, fat, neuronal, endothelial and epithelial. Due to a low abundance of mitochondria and contractile/cytoskeletal proteins, nodal cardiomyocytes are referred to as "empty" (Choudhury et al. 2015; Boyett et al. 2000).

The SN is characterised by its complex morphology and mechanisms. Therefore, to bring more fun to the "funny" journey, we aimed to: use next generation sequencing (NGS) to identify other key unexplored 'novel' TFs in the human SN vs. RA; use ingenuity pathway analysis (IPA) to identify predicted interactions amongst 'novel' TFs and 'embryonic' TFs (well known to be involved in the embryonic development of the SN) described by (van Eif et al., 2018) and identify any predicted interactions amongst key TFs with those genes involved in pacemaker mechanisms - especially the funny channel; determine the expression of key markers of different cells type as well as organelles in the SN vs. RA and identify any predicted interactions amongst TFs and markers; identify predicted interactions of TFs, markers and recently published key miRs (Petkova et al., 2020).

The dysfunction of the two clock pacemaker mechanisms as well as changes to tissue morphology (e.g., in fibrosis) contribute to the development of sinus node dysfunction (SND), which is characterised by tachycardia and bradycardia, sinus pauses, sinus arrest, sinoatrial exit block etc – a common problem in ageing, heart failure, obesity and atrial arrythmias (Dobrzynski et al., 2013; Zhang et al., 2000).

Interestingly, is has recently been shown, that in severe COVID-19 patients who suffer from bradycardia (Amaratunga et al., 2020; Capoferri et al., 2020), miR-486-3p is shown to be elevated in their RBC-depleted whole blood due to immune system response (Tang et al., 2020). Furthermore, in the mouse atrioventricular node (AV node), an unusually high expression of immune cells (such as macrophages) has been discovered by (Hulsmans et al., 2017). They noticed that depletion of macrophages in mice results in AV block and bradycardia (Hulsmans et al., 2017). They also noticed that HCN4-expressing cardiomyocytes in the AV node frequently intersperse with macrophages (Hulsmans et al., 2017). Could this upregulation of circulating miR-486-3p in the coronavirus disease 2019 (COVID-19) patients lead to downregulation of HCN4 hence reduced heart rate via immune response?

This study seeks to contribute further to our understanding of the morphological, molecular and functional characteristics of the human heart's primary pacemaker and we hope that this will set a scene for this funny journey to continue for 40 more years and beyond, and thus provide new insight into the treatment of SND.

2. Materials and methods

2.1. Specimens' information

Human specimens were obtained, dissected and frozen by co-authors in Romania (FP) and Australia (PM) under their local ethical approval procedures. Specimens from Australia (Table 1, specimens 6, 7, 10) were obtained for research from hearts that were unsuitable for heart transplantation (Ethics Approval EC256, The Prince Charles Hospital Ethics Committee). Written authorisation for removal and use of tissue was obtained from the available Senior Next of Kin. Post-mortem specimens from Rumania (Table 1, specimens 2–5, 8, 9) were from suicide and road traffic accidents people and no informed consent was required for FP to remove and use the tissue for research. After transfer to the University of Manchester, specimens were stored under the Human Tissue Act 2004. The age of patients ranged between 19 and 54. Further information can be found in Table 1 and in (Petkova et al., 2020). The quality and quantity of RNA was also assessed in (Petkova et al., 2020).

2.2. Sectioning and histology

Ten frozen tissue blocks were sectioned perpendicular to the crista terminalis and superior vena cava (SVC) and cryosections were 10–30 μm thick.

Masson's trichrome histological staining was used to confirm the location of the SN. This is our preferred staining method for the SN identification, because nodal cells (stained purple) are embedded into significant amounts of connective tissue (stained blue) as previously described (Chandler et al., 2009) and can be seen in Fig. 1A–C.

Table 1
Patient information.

Specimen Number	Patient Age	Patient Gender	Cause of death
1	29	M	Road accident
2	22	M	Road accident
3	66	M	Suicide
4	19	M	Suicide
5	60	M	Sudden death
6	54	M	Intracranial haemorrhage
7	42	M	Subarachnoid haemorrhage
8	19	M	Suicide
9	21	M	Suicide
10	54	M	Intracranial heamorrhage

2.3. Next generation sequencing for mRNA and qPCR for miRs

Ten SN samples were collected from the area around the SN artery (Fig. 1) and RA samples from the pectinate muscles remote from the SN region as described by (Petkova et al., 2020). NGS for RNA-sequencing (RNA-seq) was performed on RNA samples from 3 SN, 3 RA (Table 1, specimens 8, 9, 10) and qPCR for miRs was performed on RNA samples from 7 SN, 7 RA (Table 1, specimens 1–7) as described in our recently published study (Petkova et al., 2020).

We used Bcl2fastq software (2.17.1.14) to generate mRNA expression database for the SN vs. RA as individual values as well as mean values, Log2fold change, P values, adjusted P values and calculated percent as shown in Table 2 – 4 from the SN and RA specimens. Our published principal component analysis confirmed the SN samples are similar and different from RA samples (Petkova et al., 2020).

2.4. Bioinformatics

2.4.1. Ingenuity Pathway Analysis

The Ingenuity Pathways Analysis (IPA; Ingenuity systems, Qiagen) knowledge-base contains information about experimentally validated genes, origin and function of which can be found in the published scientific literature and other databases such as TarBase, miRBase (http://www.mirbase.org/), Genome (https://genome.ucsc.edu), RNA22 (https://cm.jefferson.edu/rna22/) and TargetScan Human (http://www.targetscan.org/). Identification of the transcription factors/transcription regulators (TFs), which were significantly more expressed (log2 fold change>1), or significantly less expressed (log2 fold change < −1) in the SN vs. RA in our data set was performed using IPA software. Our NGS dataset that was uploaded into IPA and contained the gene ID of 2595 mRNAs significantly less or more expressed in the SN vs. RA, gene ID, base mean values ('experimental intensity'), log2fold change ('experimental log ratio'), P value ('experimental P-value') and adjusted P value ('Padj'). The uploaded dataset was 'analysed/filtered' by performing 'Core Analysis' to compare our dataset to IPA knowledge base. This allowed us to identify 1424 mRNAs significantly more/less expressed mRNAs in the SN vs. RA within our data set. A Log2foldchange cut-off of −1.5 to 1.5 was selected in order to narrow down and select only significantly expressed molecules in our dataset.

In order to identify TFs from 1424 significantly more/less expressed mRNAs in the SN vs. RA, within IPA, we selected the 'transcription regulator' option from the 'molecule type' drop-down menu and performed analysis. We identified 68 TFs that were significantly more expressed in the SN vs. RA and 60 TFs that were significantly less expressed in the SN vs. RA (see Tables 2 and 3).

After identifying all 128 differentially expressed TFs, we were interested in investigating how these TFs regulate different cell types and organelles in the SN vs. RA. In order to do this, key markers for each cell types and organelles (see Table 4) were selected from our NGS dataset, based on their gene description. The estimation of NGS-based expression of key markers was correlated with the TFs pattern. In total, 48 key markers were selected from our NGS dataset (Table 4). The reliability of selected genes as markers of each cell type and/or organelles (see Results section for further information) was confirmed on the basis of published literature and IPA data).

2.4.2. Creating and analysing interactions/networks in IPA

For each TF identified, individual pathways' network was created. In total 128 individual pathways were created and predicted targets ranged in individual networks from 0 to 153. Out of 128 only 27 TFs were identified to show interactions amongst each other. We also searched for interactions of 27 TFs with 48 selected markers of cells/organelles and 11 TFs were identified as directly

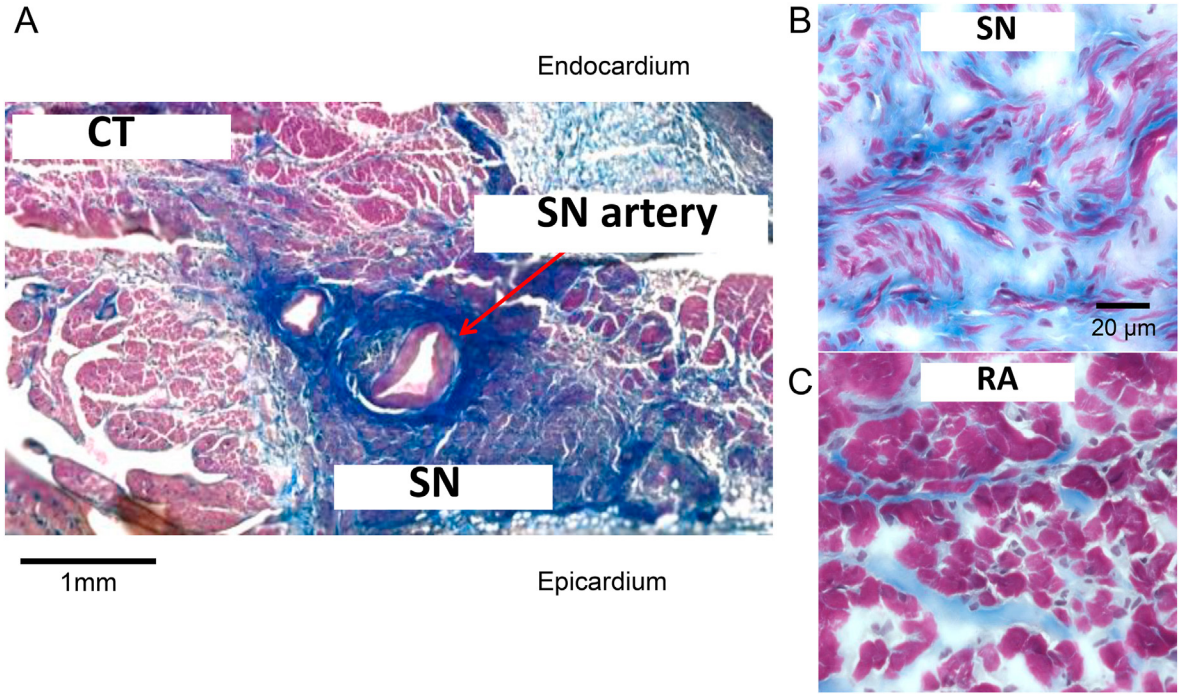

Fig. 1. Morphology of the sinus node in comparison to right atrium. A, Masson trichrome stained section through the sinus node showing nodal myocytes around the sinus node artery. Myocytes are stained purple and connective tissue is stained blue. The sinus node tissue is evident by the extensive connective tissue region. **B** and **C,** closer view of the sinus node (B) and right atrium (C). CT = crista terminalis; SN = sinus node.

Table 2
Transcription factors that significantly more expressed in the sinus node vs. right atrium. The table shows gene names of 68 transcription factors; expression in the SN and RA ± SEM; log2foldchange; adjusted P value (all calculated using the Bcl2fastq software 2.17.1.14); and % of each transcription factor in the SN/RA (where 100% expression is in the RA).

Transcription factor (gene name)	SN mean	SN ± SEM	RA mean	RA ± SEM	Log2fold change	Adjusted P value	% (SN/RA)
AKNA	677.906	142.210	319.611	57.408	1.055	1.134E-03	47.147
ATF5	540.281	69.534	247.840	41.619	1.127	1.312E-03	45.872
BACH2	226.331	59.842	97.960	20.395	1.130	9.556E-03	43.282
BATF	61.748	22.495	11.799	6.641	2.674	3.648E-04	19.109
BCL11B	39.23	22.307	8.633	6.676	2.608	5.776E-03	22.006
CEBPA	282.356	65.316	52.355	24.256	2.653	1.464E-08	18.542
CERS5	896.236	87.785	433.370	61.242	1.054	1.014E-03	48.354
CIITA	398.745	111.455	149.505	36.256	1.381	7.075E-05	37.494
DLX1	108.905	48.375	20.363	11.822	2.433	1.883E-04	18.698
DLX2	48.099	20.607	8.451	4.757	2.738	2.228E-03	17.570
DTX1	249.000	39.096	74.937	20.187	1.793	8.086E-06	30.095
FOXD3	385.436	175.537	84.572	47.553	2.199	5.883E-07	21.942
GLI1	183.878	38.227	57.936	7.130	1.607	1.140 E−03	31.508
GLI2	347.127	75.203	137.196	19.863	1.283	3.754E-03	39.523
HDAC10	38.406	10.630	6.879	1.777	2.465	4.688E-03	17.912
HEY2	457.506	13.418	165.326	11.391	1.463	1.335E-05	36.136
HIC1	1362.142	353.431	521.178	112.365	1.323	1.587E-05	38.262
HLX	782.153	165.116	306.64	117.080	1.468	1.079E-05	39.205
HOXA3	122.178	35.992	18.937	3.932	2.610	6.601E-06	15.500
HOXA5	61.832	13.331	12.492	4.679	2.387	6.226E-04	20.203
HOXB2	776.382	153.160	166.100	53.351	2.319	1.204E-12	21.394
HOXB3	440.507	40.289	76.885	29.006	2.722	1.332E-10	17.454
HOXB4	221.93	24.513	37.187	24.114	3.091	1.103E-08	16.756
HOXC4	107.812	34.363	15.536	3.518	2.723	1.052E-06	14.411
HOXD8	85.567	7.471	26.220	9.035	1.852	3.520E-03	30.642
HR	419.256	156.295	151.074	40.595	1.249	3.728 E−03	36.034
IER2	5491.416	1798.91	2118.285	678.573	1.361	6.376E-07	38.574
IKZF1	189.948	118.644	46.666	22.659	1.792	9.265E-05	24.568
IRF7	493.157	124.674	213.957	75.260	1.256	4.397E-04	43.385
ISL1	208.879	83.062	0.000	0.000	12.140	9.242E-05	0.479
KCNIP3	389.946	148.584	138.006	68.334	1.607	6.986E-06	35.391
KLF2	6750.78	1240.935	2732.485	295.238	1.253	1.599E-05	40.477
LBH	2394.91	443.351	1091.937	135.245	1.093	4.424E-03	45.594
LMO2	687.174	86.682	319.748	115.363	1.280	5.251E-03	46.531
LYL1	379.379	41.071	181.422	9.254	1.038	6.576E-03	47.821
LZTS1	234.963	59.310	76.747	13.548	1.572	2.987E-04	32.664
MAF	1475.905	276.728	548.679	102.208	1.418	1.014E-06	37.176
MEOX1	1350.634	629.078	662.000	360.592	1.108	3.625E-04	49.014
MLXIPL	234.667	80.361	79.937	22.441	1.522	5.286E-04	34.064
MSC	1603.090	546.664	490.110	191.398	1.798	1.287E-09	30.573
MYCN	61.499	5.4330	10.308	4.002	2.689	2.365E-04	16.762
NFKBIZ	870.258	184.484	329.93	38.444	1.338	9.408E-04	37.912
NLRC5	341.150	66.534	136.747	23.483	1.303	4.248E-04	40.084
NUPR1	5710.273	179.142	2548.803	440.630	1.199	1.857E-04	44.635
PHOX2B	74.570	23.194	10.887	6.165	3.131	3.272E-05	14.600
PRDM16	456.732	25.624	137.165	9.657	1.727	6.020E-07	30.032
PYCARD	301.691	77.164	101.776	6.302	1.475	2.029E-04	33.735
RUNX1	412.141	61.976	112.900	13.806	1.841	1.892E-06	27.393
RUNX2	101.047	16.069	25.667	3.726	1.959	4.618E-04	25.401
RUNX3	97.062	41.225	25.676	14.122	2.041	3.027E-04	26.453
SHOX2	1039.710	260.04	223.735	78.368	2.250	1.719E-08	21.519
SMARCD2	1516.491	365.786	742.922	193.867	1.030	5.407E-04	48.990
SOX10	2026.732	753.631	662.197	179.093	1.394	6.052E-05	32.673
SOX13	1369.973	110.721	631.294	47.328	1.104	2.6400E-04	46.081
SOX17	584.337	39.839	290.279	85.723	1.101	2.817E-03	49.677
SOX2	153.772	53.947	21.604	6.022	2.776	1.521E-08	14.049
SOX9	3348.057	108.482	1507.809	373.240	1.231	5.124E-04	45.035
SPI1	381.480	186.713	119.83	69.676	1.799	5.273E-07	31.412
SREBF1	4927.952	1336.040	2308.654	325.077	1.001	1.191E-03	46.848
TBX1	131.445	67.297	36.094	25.787	2.261	2.286E-03	27.459
TBX18	1190.75	86.23333	470.920	64.5568	1.345	4.956E-05	39.548
TBX2	1749.702	175.142	658.368	122.010	1.434	8.247E-05	37.627
TBX3	1972.733	469.804	543.995	115.281	1.845	7.316E-07	27.576
TGFB1I1	2466.217	284.716	872.904	75.898	1.477	1.511E-06	35.394
TSC22D3	9758.316	3669.472	4380.536	1004.956	1.030	2.313E-03	44.891
TWIST1	377.545	84.672	143.105	42.079	1.470	9.327E-05	37.904
VAV1	107.197	57.514	24.553	11.685	1.912	3.517E-03	22.904
VENTX	98.187	15.838	10.922	3.750	3.294	7.27E-08	11.123

Table 3
Transcription factors significantly less expressed in the sinus node vs. right atrium. The table shows gene names of 60 transcription factors; expression in the SN and RA ± SEM; log2foldchange; adjusted P value (all calculated using the Bcl2fastq software 2.17.1.14); and % of each transcription factor in the SN/RA (where 100% expression in is the RA).

Transcription factor (gene name)	SN mean	SN ± SEM	RA mean	RA ± SEM	Log2fold change	Adjusted P value	% (SN/RA)
ACTN2	21634.431	7833.845	59256.856	5474.155	−1.662	1.398E-04	36.510
ASB15	123.674	37.790	1739.861	474.424	−3.848	8.954E-45	7.108
ASB4	23.684	6.879	70.022	13.042	−1.645	8.560 E−03	33.824
ASB5	16.300	7.161	133.294	23.129	−3.233	4.37E-09	12.228
ASB8	637.596	50.060	1291.190	48.396	−1.037	7.061E-04	49.380
BRCA1	126.173	10.455	282.040	60.510	−1.120	4.219E-03	44.736
CAND2	590.303	136.063	1630.819	216.947	−1.539	4.103E-07	36.197
CASKIN1	98.435	21.743	370.275	36.706	−1.973	1.854E-06	26.584
CBX4	602.128	129.064	1333.066	241.324	−1.186	5.616E-04	45.169
CERS6	1222.011	380.239	3551.558	784.415	−1.665	4.948E-07	34.408
CHCHD3	1259.526	186.752	2966.429	190.626	−1.273	1.240E-04	42.459
COPS5	794.737	79.793	1980.436	268.256	−1.315	5.682E-05	40.129
DCAF6	2723.082	396.688	9437.394	312.369	−1.836	7.386E-10	28.854
FEM1A	1145.289	200.935	2378.667	319.940	−1.088	1.098E-03	48.148
FHL2	4488.626	1459.722	12576.092	7584.572	−1.173	7.422E-03	35.692
GRIP1	68.755	20.714	197.073	92.005	−1.422	4.884 E−03	34.888
GTF2I	466.899	108.962	1313.898	292.866	−1.514	3.536E-07	35.535
GTF3A	2393.535	216.862	5320.791	640.947	−1.153	3.186E-04	44.985
HAND1	6.150	1.766	56.440	19.813	−3.029	9.348E-05	10.897
HDAC9	258.074	32.224	549.930	51.861	−1.112	7.917E-04	46.928
HIVEP2	538.440	57.714	1286.742	295.821	−1.201	3.419E-03	41.845
HLF	737.032	112.679	1921.831	194.315	−1.416	7.18E-07	38.350
HMGA1	420.776	54.922	856.277	41.092	−1.058	2.286E-03	49.140
HOPX	194.455	62.767	1157.648	446.288	−2.549	7.699E-18	16.797
HSF2	422.250	19.749	1691.197	128.986	−2.009	3.853E-13	24.968
KANK1	2571.452	526.933	6727.928	204.166	−1.458	1.868E-06	38.221
KAT2B	1121.328	73.391	3010.476	471.115	−1.408	1.318E-05	37.247
KCTD1	401.470	33.964	1268.950	310.905	−1.602	1.537E-06	31.638
MEF2A	2578.413	233.194	7634.998	757.997	−1.577	6.563E-09	33.771
MITF	598.513	213.906	1802.958	727.443	−1.578	7.884E-07	27.112
MKL2	956.58	331.959	2660.534	1659.107	−1.075	3.840E-04	35.954
MLIP	1407.866	431.711	6203.713	1222.175	−2.268	1.195E-13	22.694
MLX	969.099	65.291	1959.077	140.850	−1.026	4.594E-04	49.467
MYT1	3.126	2.298	32.681	10.734	−3.899	4.566E-04	9.566
NCOA2	835.154	95.142	1727.300	381.213	−1.018	1.960E-03	48.350
NCOA4	3405.760	431.596	8749.216	571.405	−1.389	4.000E-07	38.926
NFE2L1	10964.520	1829.637	28663.931	4334.959	−1.400	6.824E-07	38.252
NKX2-5	1116.112	308.341	5549.073	1761.584	−2.287	1.198E-10	20.113
NOCT	43.806	0.646	159.363	65.339	−1.663	1.464E-03	27.488
NPAS2	736.022	124.618	1503.172	308.439	−1.017	6.937E-03	48.965
PBX3	1224.393	47.244	3027.975	201.759	−1.314	5.361E-06	40.436
PPARGC1A	858.408	314.360	2627.464	651.225	−1.814	6.539E-05	32.671
PPP1R13 L	859.854	207.086	3018.562	350.626	−1.900	3.963E-10	28.486
PROX1	514.407	198.737	1897.360	415.061	−2.021	9.071E-09	27.112
RFX2	352.593	55.933	918.063	340.632	−1.133	7.258E-03	16.797
SALL1	9.075	3.795	67.701	33.401	−2.798	4.02E-04	13.405
SATB1	493.157	124.674	213.957	75.260	1.256	2.947E-04	45.573
SFMBT1	138.972	33.019	327.697	65.700	−1.285	2.152E-03	42.409
SMYD1	1604.484	589.106	5358.148	819.541	−1.960	3.263E-06	29.945
STAT4	140.858	42.809	581.692	74.953	−2.153	4.961E-08	24.215
TBX20	400.478	52.818	2094.381	304.501	−2.392	3.222E-13	19.122
TBX5	2894.793	967.928	9297.928	1916.888	−1.825	8.549E-07	31.134
TCEA3	828.140	135.026	1736.017	182.424	−1.098	9.300E-04	47.703
TEAD1	2063.731	110.694	4656.889	513.296	−1.174	6.386E-05	44.316
TRIM24	400.102	64.223	875.524	95.024	−1.160	3.398E-04	45.699
VGLL2	32.552	29.600	60.589	25.769	−2.293	5.569E-03	43.727
YAF2	766.448	115.140	1719.524	37.999	−1.211	1.716E-04	44.573
YBX3	6104.641	277.970	13980.831	1611.231	−1.191	2.562E-05	43.664
ZBTB20	158.281	30.758	626.103	388.802	−1.494	7.478E-04	25.280
ZNF189	453.549	22.899	1185.676	426.572	−1.228	1.061E-03	38.252

interacting with 6 different key markers. In addition, we identified those TFs that directly and/or indirectly regulate the key genes involved in pacemaking.

Previously we predicted 15 miRs, which interact with the key molecules involved in the SN's pacemaking (Petkova et al., 2020). Therefore, we were interested if these key 15 miRs interact with differentially expressed TFs and markers. The interaction for 27 TFs and 48 markers with 15 miRs was tested using IPA and identified interaction is shown in Table 5.

2.4.3. Binding sites identification

For all mRNAs, the sequence of their 3′-untranslated regions (UTR) were obtained using Genome (https://genome.ucsc.edu). The sequence of all miRs were obtained using miRBase (http://www.

Table 4
Markers for different cell types and organelles expressed in the sinus node vs. right atrium. The table shows gene names of markers (see Fig. 11); expression in the SN and RA ± SEM; log2foldchange; adjusted p value (all calculated using the Bcl2fastq software 2.17.1.14); and % of each marker in the SN/RA (where 100% expression in the RA).

Marker (gene name)	SN mean	SN ± SEM	RA mean	RA ± SEM	Log2fold change	Adjusted P value	% (SN/RA)
ACTG2	1242.990	432.331	269.4733	41.119	2.050	3.678E-08	461.266
ACTN2	21634.430	7833.845	59256.86	5474.156	−1.662	1.398E-04	36.510
CD209	219.460	125.490	76.090	50.976	1.581	5.850E-04	288.436
CD44	2595.847	604.517	1277.290	291.791	1.035	2.819 E−03	203.230
CERCAM	3012.570	893.747	1013.453	329.419	1.550	9.575E-08	297.258
COL14A1	9472.997	1597.945	4242.62	953.404	1.183	1.971E-03	223.282
COL1A1	25501.240	4503.298	7930.85	1311.630	1.665	1.013E-09	321.545
COL1A2	58118.510	10427.945	23600.197	3021.211	1.271	1.182E-05	246.263
COL3A1	27758.890	8618.337	11647.983	2840.022	1.181	2.198E-05	238.315
COL5A1	4966.340	1553.434	2086.927	430.746	1.128	2.188 E−04	237.974
COL5A3	2761.960	915.702	1141.823	348.382	1.187	8.693E-05	241.890
COL6A1	25169.030	5652.913	12218.197	2535.694	1.025	6.598E-04	205.996
COL6A2	46818.51	6355.024	20505.690	4243.743	1.224	1.013E-04	228.320
COL8A2	600.92	163.656	197.187	34.931	1.515	8.104E-04	304.747
COL9A2	322.08	104.366	88.167	15.339	1.715	5.012E-05	365.308
COL9A3	682.560	288.143	210.997	56.040	1.390	1.507E-03	323.493
CSF1R	874.533	395.078	274.083	108.957	1.838	2.752E-09	353.943
DES	112041.9	40572.007	202808.3	17832.319	−1.141	0.0071819	55.245
DMD	2411.157	277.11	8679.833	1901.656	−1.808	4.415E-08	27.779
EMILIN1	3317.597	360.138	1381.06	302.828	1.316	2.127E-05	240.221
FABP4	1802.743	350.257	316.377	79.730	2.539	9.571E-11	569.809
GZMA	59.184	41.363	8.052	2.872	2.387	3.830E-04	735.000
HLA-DMA	829.197	77.720	328.510	65.641	1.369	2.325E-05	252.411
HLA-DMB	197.270	34.208	64.797	13.501	1.620	2.046E-04	304.445
HLA-DOA	281.580	59.060	78.817	18.096	1.849	1.412E-06	357.259
HLA-DPA1	3574.673	333.741	1565.163	94.958	1.172	6.401E-05	94.958
HLA-DPB1	2027.295	407.980	931.253	128.927	1.275	1.321E-05	217.695
HLA-DQA1	672.007	98.565	231.413	39.456	1.535	1.76E-06	290.392
HLA-DQB1	1358.700	119.051	592.570	82.459	1.202	2.075E-04	229.289
HLA-DRA	4667.940	808.427	2002.060	235.036	1.182	6.295E-05	233.157
HLA-DRB1	4042.847	630.230	1702.450	104.091	1.202	5.656E-05	237.472
HLA-DRB5	1214.300	777.612	520.970	302.671	1.128	6.960E-04	233.084
INA	61.443	18.434	7.337	6.157	3.770	1.962E-04	837.483
MRPL15	1129.537	234.793	2254.08	289.964	−1.044	7.607E-03	50.111
MRPL33	1310.670	180.021	2891.307	306.905	−1.161	5.854E-04	45.331
MRPL35	1054.260	163.380	2374.223	25.602	−1.220	1.458E-04	44.404
MRPL39	449.207	36.865	985.8433	149.484	−1.118	9.678E-04	45.5666
MRPL50	540.197	47.376	1071.587	32.518	−1.009	1.225 E−03	50.411
MRPS23	674.4633	103.967	1396.073	128.115	−1.081	5.398E-04	48.311
MRPS30	667.847	79.874	1635.447	133.496	−1.316	7.679E-06	40.836
MRPS33	721.797	49.514	1461.570	210.658	−1.005	3.432E-03	49.385
MRPS36	539.670	44.411	1313.953	210.581	−1.264	2.877E-03	41.072
MRPS9	865.430	123.524	1804.787	260.927	−1.070	4.472E-03	47.952
MUC1	99.317	24.787	29.730	7.725	1.710	1.691E-03	334.062
MYH6	217807.900	83862.528	1066895.000	115574.238	−2.528	7.279E-13	20.415
TNNT2	52996.690	15892.935	144599.200	21446.601	−1.560	1.099E-04	36.651
TPSAB1	408.170	60.284	54.140	5.871	2.889	1.147E-16	753.916
TTN	27820.200	8702.962	154512.700	72399.518	−2.376	5.388E-08	18.005

mirbase.org/). The sequence of the miRs and their predicted target mRNAs were uploaded into RNA22 (https://cm.jefferson.edu/rna22/) or TargetScan Human (http://www.targetscan.org/). The number of miRs binding sites on their predicted mRNAs is summarised in Table 5.

2.4.4. Heat maps

Heat maps were created using Heatmapper (http://www.heatmapper.ca/expression/). To do this, a dataset containing gene names and the normalised count of each gene expressed in each SN sample (n = 3, Tables 2–4) or RA sample (n = 3, Tables 2–4) was uploaded. Greener represents higher while redder represents lower expression in the SN vs. RA. Z-score of −1 indicates that a sample is one standard deviation below the mean value; and a Z-score of 1 indicates a sample is one standard deviation above the mean value (see Tables 2–4 for mean values).

2.4.5. Graphs and statistical analysis

GraphPad Prism 8.4.3. software was used for statistical analysis and for making graphs. Data are shown as mean ± SEM in Tables 2–4 and graphs are plotted as % SN/RA. Significant differences were identified with one-way ANOVA test; differences were assumed as significant at $P < 0.001$.

3. Results

3.1. The sinus node region is characterised by extensive connective tissue and fewer myocytes

To confirm the location of the SN, Masson's trichrome staining was performed as shown in Fig. 1 as previously shown by (Chandler et al., 2011; Stephenson et al., 2017; Petkova et al., 2020). The SN myocytes (in purple) surround the SN artery and are embedded in a network of connective tissue (in blue).

Table 5
Predicted microRNA-transcription factor and microRNA-marker interactions. This data is based on the expression of microRNAs from our previous study by Petkova et al. (2020) and the expression of transcription factors and markers from this study. From left to right, the columns show miR name; expression of each miRs in the sinus node vs. the right atrium; predicted targets according to RNA22 and TargetScan Human; expression profile of each target in the sinus node vs. the right atrium; the number of binding sites on the target according to RNA22 and TargetScan Human. Bold represents those that are upregulated in the sinus node compared to the right atrium. -, no predicted marker targets. TF = Transcription factor; HCX = Histo-compatibility complex. All predicted interactions from IPA were chosen for this table that were functionally validated.

miRNA	miRNA expression in SN vs. RA based on Petkova et al. (2020)	Gene name of predicted target	mRNA expression based on this study	Total no. of binding sites for each miRNA on predicted target P<0.05 and P>0.05
hsa-miR-10b-5p	↑	TBX5 (TF)	↓	1
hsa-miR-30c-5p	↓	**COL1A1 (Collagen)**	↑	0
		RUNX2 (TF)	↑	2
		COL1A2 (Collagen)	↑	0
		COL9A3 (Collagen)	↑	1
		COL5A1 (Collagen)	↑	0
hsa-miR-133a-3p	↓	**COL1A1 (Collagen)**	↑	1
		RUNX2 (TF)	↑	0
		HLA-DOA (HCX)	↑	0
		TPSAB1 (Mast cells marker)	↑	1
		COL9A2 (Collagen)	↑	0
hsa-miR-153-3p	↑	MITF (TF)	↓	1
		MEF2A (TF)	↓	1
		PPARGC1A (TF)	↓	1
hsa-miR-215-5p	↑	NKX2-5 (TF)	↓	1
hsa-miR-422a	↓	**TBX3 (TF)**	↑	2
		GLI2 (TF)	↑	3
hsa-miR-429	↓	**SOX2 (TF)**	↑	1
hsa-miR-486-3p	↓	**LBH (TF)**	↑	1
		LZTS1 (TF)	↑	12
		SOX13 (TF)	↑	3
		CERCAM (Endothelial cell marker)	↑	1
		TPSAB1 (Mast cell marker)	↑	2
		CD209 (Macrophage cell marker)	↑	1
		HLA-DRA (HCX)	↑	2
		HLA-DRB5 (HCX)	↑	1
		HLA-DRB1 (HCX)	↑	1
hsa-miR-512-5p	↑	NKX2-5 (TF)	↓	0
hsa-miR-938	↓	**LBH (TF)**	↑	2
		SOX2 (TF)	↑	2
hsa-miR-1225-3p	↑	NKX2-5 (TF)	↓	2
hsa-miR-483-3p	↓	**LBH (TF)**	↑	1
hsa-miR-1-3p	↓	–	–	–
hsa-miR-198	↑	–	–	–
hsa-miR-204-5p	↑	–	–	–

3.2. Identification of 'novel'/unexplored transcription factors in the sinus node vs. right atrium

Tables 2 and 3 list all transcription factors (TFs) that are significantly more or significantly less expressed in the SN vs. RA. Using IPA, we have identified 68 significantly more expressed and 60 significantly less expressed TFs in the SN vs. RA. The position of these TFs is shown in Fig. 2 (A, B) on Volcano plots. Most identified TFs are within a range of 0 to +5 or 0 to −5 log2Foldchange with the exception of ISL1 (well known to be involved in the embryonic development of the SN) which is > 10 log2Fold change.

The heat maps in Figs. 3A and 4A show expression profiles of TFs in individual SN and RA samples. As expected, there is some inter-individual variation in the expression of TFs within the range of 0−1 and 0 to −1 Row Z-score.

TF expression profiles are shown as percent in the SN/RA (Figs. 3B and 4B and Tables 2 and 3). It is interesting to observe that ISL1 is the most abundant TF in the adult human SN (Fig. 3B). Amongst well known TFs (important for the embryonic development of the SN), TBX3 and SHOX2 are highly expressed in the adult SN compared to other TFs. Many 'novel'/unexplored TFs in the adult SN, were identified to be highly expressed e.g., FOXD3 (known to regulate cardiac neural crest progenitors in the mouse heart - (Nelms et al. 2011), DLX2 (known to regulate lymphocyte development - (Sunwoo et al., 2008), PHOX2B (known to be associated with congenital heart disease in humans (Lombardo et al., 2018), VENTX (known to promote myeloid cell differentiation that may differentiate into macrophages (Leitoguinho et al., 2019), SOX2 (known to be involved in stem cell preservation and self-renewal (Mallanna et al., 2010) and a few HOX-TFs members (e.g. HOXA3, HOXB4 and HOXC4) that play a major role in heart development and are highly relevant to human pathology (Lescroart and Zaffran 2018).

Interestingly, NKX2-5 and TBX5 (key embryonic TFs) are <50% expressed in the adult human SN vs. RA (Fig. 4B). Amongst 'novel' TFs that are least abundant in the human SN are ASB5 and ASB15

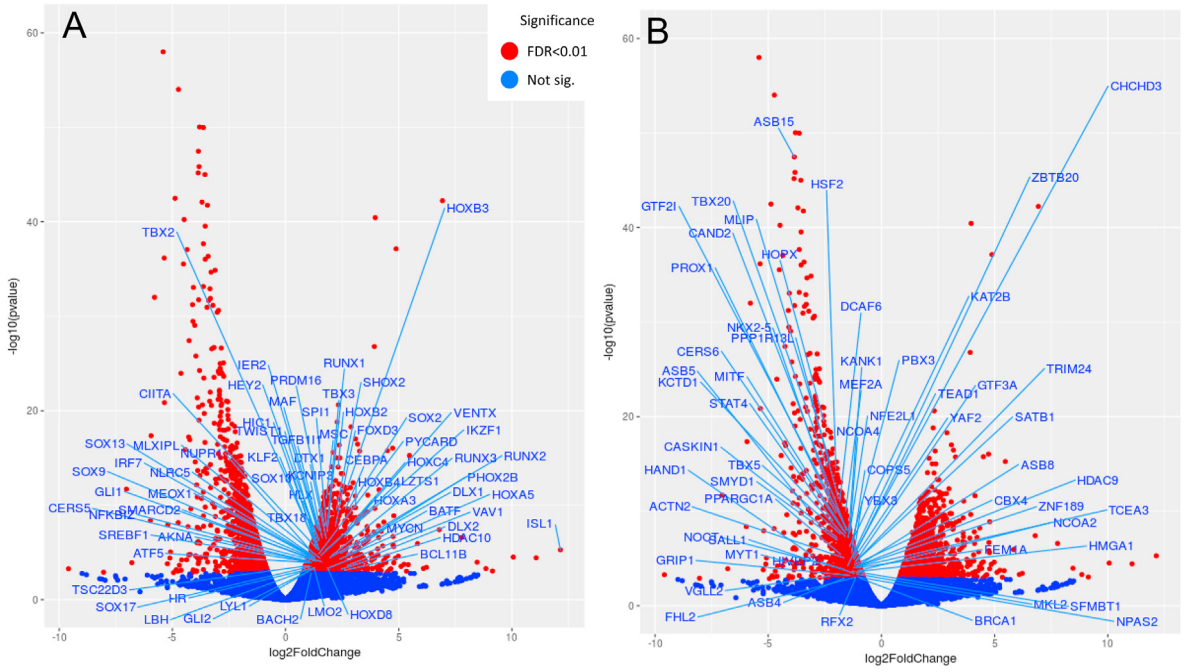

Fig. 2. Volcano plot of significantly more and significantly less expressed transcription factors in the sinus node vs. right atrium. A, location of 68 transcription factors that are significantly more highly expressed in the sinus node compared to right atrium. **B,** location of 60 transcription factors that are significantly less expressed in the sinus node, compared to the right atrium. See Tables 1 and 2 for details. Red = significantly more/less expressed mRNA; blue = non-significantly expressed mRNAs.

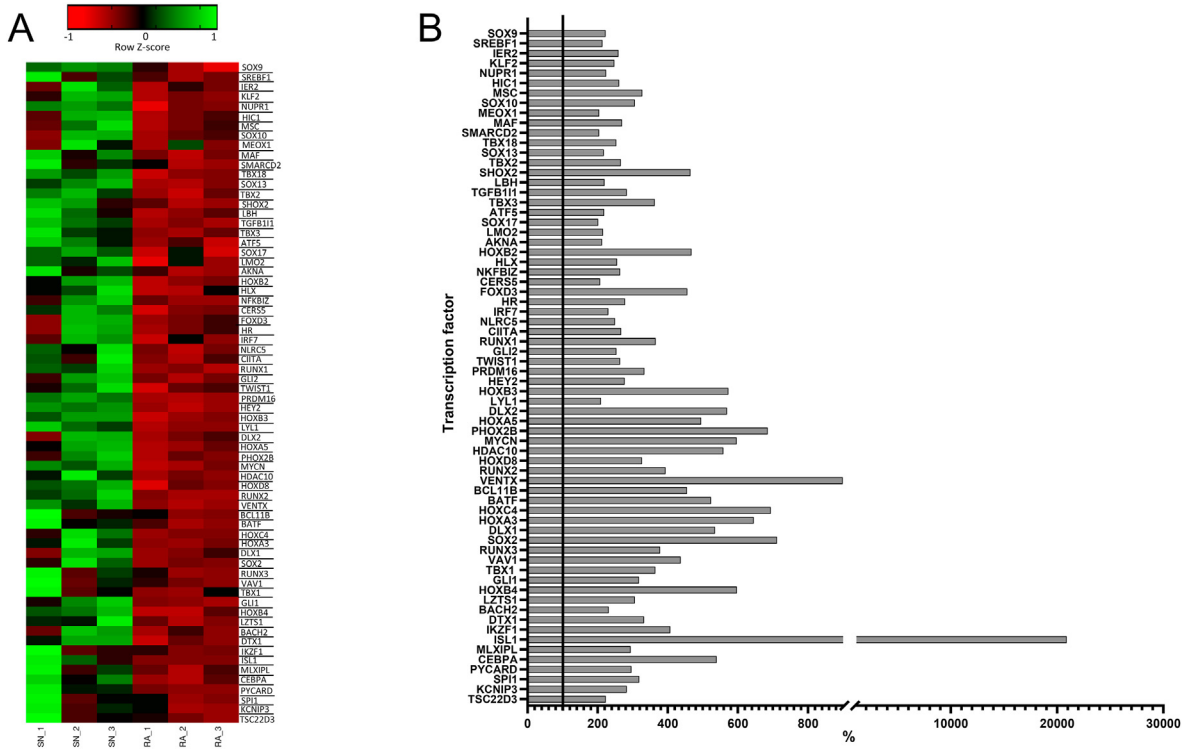

Fig. 3. Expression profile of 68 transcription factors that are significantly more expressed in the adult human sinus node vs. right atrial muscle. A, heat map shows inter-individual expression of each transcription factor in each sinus node (SN1 – SN3) and right atrium (RA1 – RA3) samples. **B,** mean expression of transcription factors in the sinus node vs. right atrium (n = 3) plotted as % SN/RA (see Table 2 for details). The black line at 100% represents the transcription factors expression in the right atrium (i.e., basal level). SN = sinus node; RA = right atrium.

(known to be associated with skeletal muscle growth (McDaneld et al. 2004) MYT1, known to promote neuronal cell differentiation, (Vasconcelos et al., 2016); HAND1, known to be associated with cardiac cell differentiation, (Riley et al. 1998); SALL1, known to be associated with early heart development, (Morita et al., 2016); RFX2 (known to maintain brain development HOPX (known to

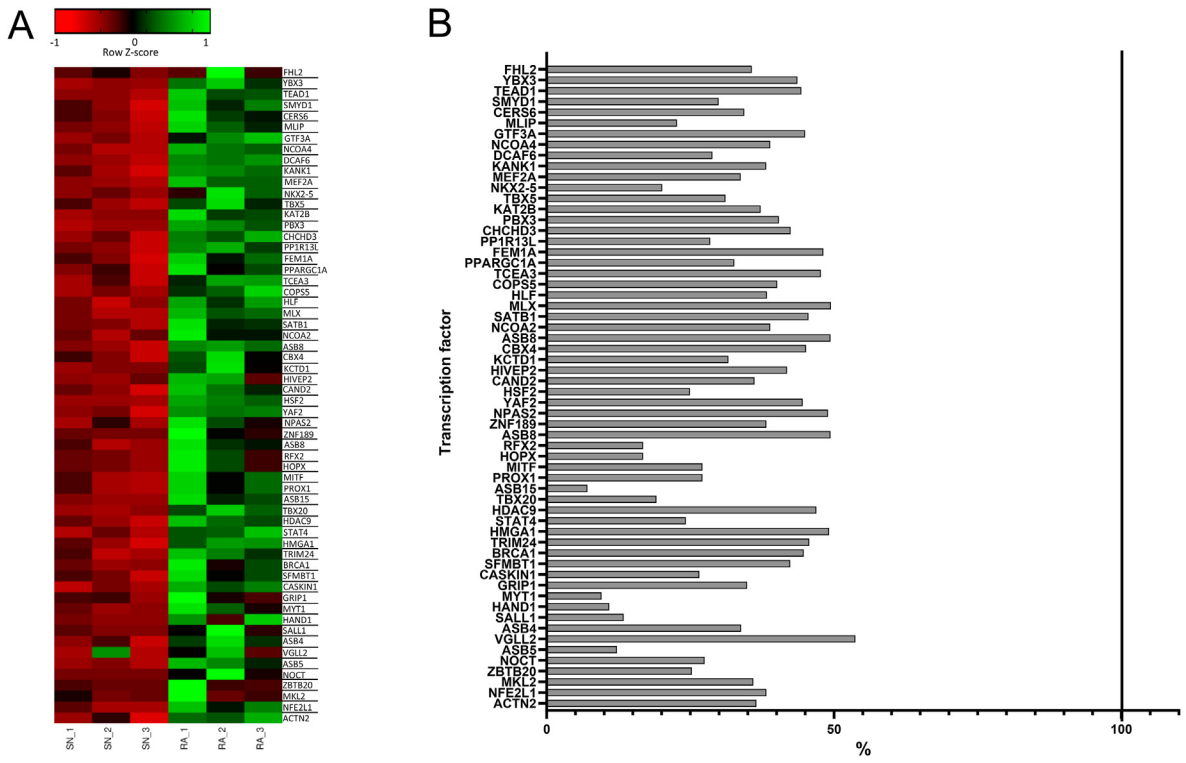

Fig. 4. Expression profile of 60 transcription factors that are significantly less expressed in the adult human sinus node compared vs. right atrial muscle. A, heat map shows inter-individual expression of each transcription factor in each sinus node (SN1 – SN3) and right atrium (RA1 – RA3) samples. **B,** mean expression of transcription factors in the sinus node vs. right atrium (n = 3) plotted as % SN/RA (see Table 3 for details). The black line at 100% represents the transcription factors expression in the right atrium (i.e., basal level). SN = sinus node; RA = right atrium.

regulate hypertrophy and maturation of cardiomyocytes (Friedman et al., 2018) (Fig. 4B).

3.3. Prediction of interactions amongst transcription factors and their predicted role in regulating HCN4 and Ca^{2+} proteins

One of the main aims of this study was to predict the interaction of the key 'novel' TFs with each other and with TFs known to be involved in the embryonic development of the heart (ISL1, TBX3, TBX5, NKX2-5, SHOX2) as well as to gain further insight into their relationship with HCN4 and Ca^{2+} handling proteins (RYR2, Na^{2+}-Ca^{2+} exchanger, NCX1 and SERCA2A). An example of IPA-based interaction network is shown in Fig. 5 which includes well known TFs. ISL1 and TBX3 facilitate while NKX2-5 and TBX5 inhibit the expression of HCN4, and Ca^{2+} channels, $Ca_V3.1$ and Cav3.1, (Park and Fishman 2017). HCN4, RYR2, NCX1 and SERCA2A have previously been shown by our group to be differentially expressed in the SN vs. RA (Chandler et al., 2011): HCN4 more and both RYR2 and SERCA2A less expressed in the adult human SN vs. RA.

Using IPA, we can appreciate the complexity of interactions of many TFs that can directly and/or indirectly control the function of the pacemaker of the heart. IPA analysis revealed that besides HCN4, ISL1 (the most abundant TF in our adult human SN) activates 'novel' TFs RUNX3 (known to maintain the differentiation of mesenchymal cells during heart development (Fu et al., 2011) and RUNX1 (known to be involved in cardiac repair following myocardial infarction (McCarroll et al., 2018). Oppositely, ISL1 is activated by RUNX2 (known to be involved in osteoblast differentiation (Alfieri et al., 2010), whereas GLI1 (known to regulate the coordination of the heart and lung (Park et al., 2000)) activates RUNX2 and SOX2 (Figs. 5A and 3B) activates TBX3. Together they activate the expression of HCN4. Interestingly, the most targeted TF is RUNX2 with 6 activators (Fig. 5A).

Out of those TFs that are less abundant in the SN but more abundant in the RA, TBX5 is shown to interact with NKX2-5 and HOPX (one the novel TFs to be least expressed in the adult human SN (Figs. 4B and 5B). TBX5 activates NCX1, RYR2 and SERCA2A and NKX2-5 activates RYR2 (Fig. 5B). MEF2A (another novel TF more abundant in the adult human RA, known to regulate the mammalian cardiomyocyte differentiation (Desjardins and Naya 2016), like TBX5, activates SERCA2A (Fig. 5B). MEFA2A also activates ASB4 (known to be expressed in murine embryonic vasculature (Bode et al., 2011) and PPARGC1A (a regulator of mitochondrial biogenesis (Duncan and Finck 2007) (Fig. 5B).

3.4. Markers for key cell types and organelles more abundant in the sinus node compared to the right atrium

Fig. 1 shows the SN is characterised by more connective tissue than surrounding RA. We therefore aimed to identify other cell types' markers that are present within its connective tissue. From our NGS dataset we identified, and then selected at least one marker of each cell type: ACTG2 for the smooth muscle cells (Wangler et al., 2014); CSF1R and CD209 for macrophages (Rojo et al., 2019) (Ortiz et al., 2008); FABP4 for fat/adipocytes cells (Queipo-Ortuno et al., 2012); INA for neuronal cells (Baum and Garriga 1997); MUC1 for epithelial cells (Dhar and McAuley 2019); TPSAB1 for mast cells (Lyons et al., 2017); CERCAM for endothelial cells (Starzyk et al., 2000); COL1A1 for fibroblasts (Wong et al., 2020); CD44 for mesenchymal stem cells (Maleki et al., 2014), widely investigated for many therapies including creation of a biological pacemaker (Hu et al., 2019); GZMA for natural killer cells (Cursons et al., 2019) and EMILIN1 for elastic fibres (Zanetti et al., 2004).

Table 4 lists markers and their mean ± SEM expression profile in 3 SN and 3 RA. The heat map shows their expression profile in each

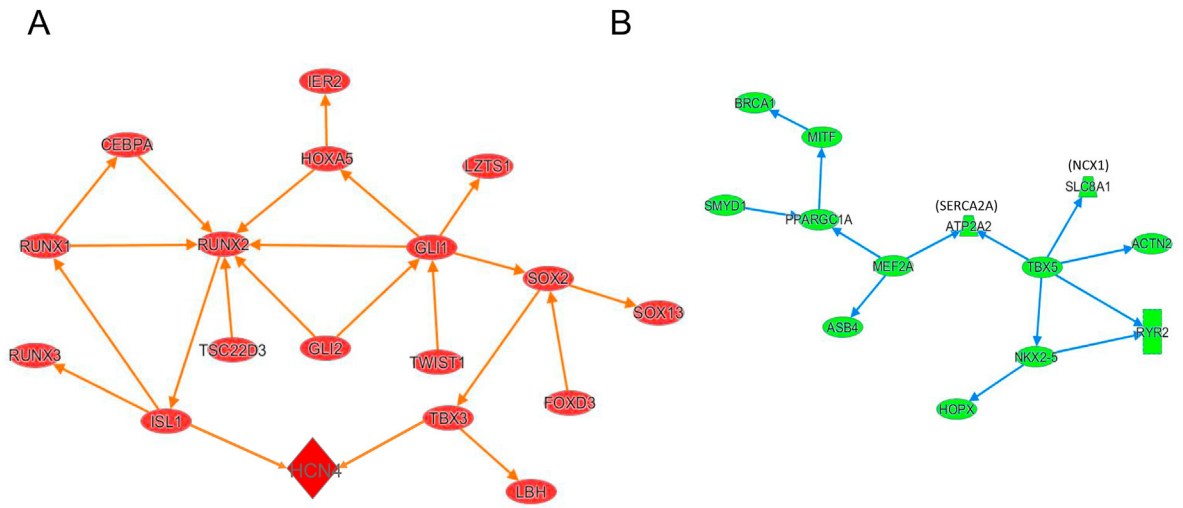

Fig. 5. Ingenuity Pathway Analysis predictions of interactions amongst 'novel' and well-known transcription factors (to be involved in embryonic development of the heart) and their predicted role in controlling HCN4 and Ca^{2+} handling proteins. A, transcription factors that were more abundant in the sinus node vs. right atrium. **B,** transcription factors that were less abundant in the sinus node vs. right atrium. Arrows = predicted activation. Oval shape = transcription factors; trapezoid shape = calcium-handling proteins; diamond shape = HCN4, hyperpolarisation-activated neuclotide-gated channel 4; NCX1 = Na^{+}/Ca^{2+} exchanger; SERCA2A = sarcoplasmic reticulum Ca^{2+}-ATPase. Red nodes represent molecules significantly more expressed in the SN. Green nodes represent molecules that are significantly less expressed in the SN (i.e., significantly more expressed in the RA).

sample (Fig. 6A). Their expression as % SN over RA is also included in Table 4 and shown graphically in Fig. 6B. As expected, there is some inter-individual variation in the expression of these cell markers within range of 0−1 and 0 to −1 Row Z-score. Each marker is abundantly expressed in the SN samples compared to the RA (Fig. 6B). Considering that the SN is highly innervated by the autonomic nervous system (ANS) (Alboni et al., 2007) not surprisingly, the most expressed marker was INA (log2foldchange of 3.77, Table 4) and percentage difference of 837% (Fig. 6B). It was interesting to observe that the immune cell marker (TPSAB1) is highly expressed in the adult human SN (754%, Fig. 6B). Similarly to TPSAB1, the natural killer marker (GZMA) is also highly expressed in the adult human SN. In addition, the fat, smooth muscle, macrophage and mesenchymal stem cell markers are highly expressed in the human adult SN (Fig. 6B: FABP4, ACTG2, CSF1R/CD209 and CD44 are markers for these cells, respectively).

As well as the immune cells such as the mast, macrophages and natural killer being highly abundant in the adult human SN (Fig. 6), we noticed that 10 human leukocyte antigens (HLA, encoded by the major histocompatibility complex genes involved in regulation of

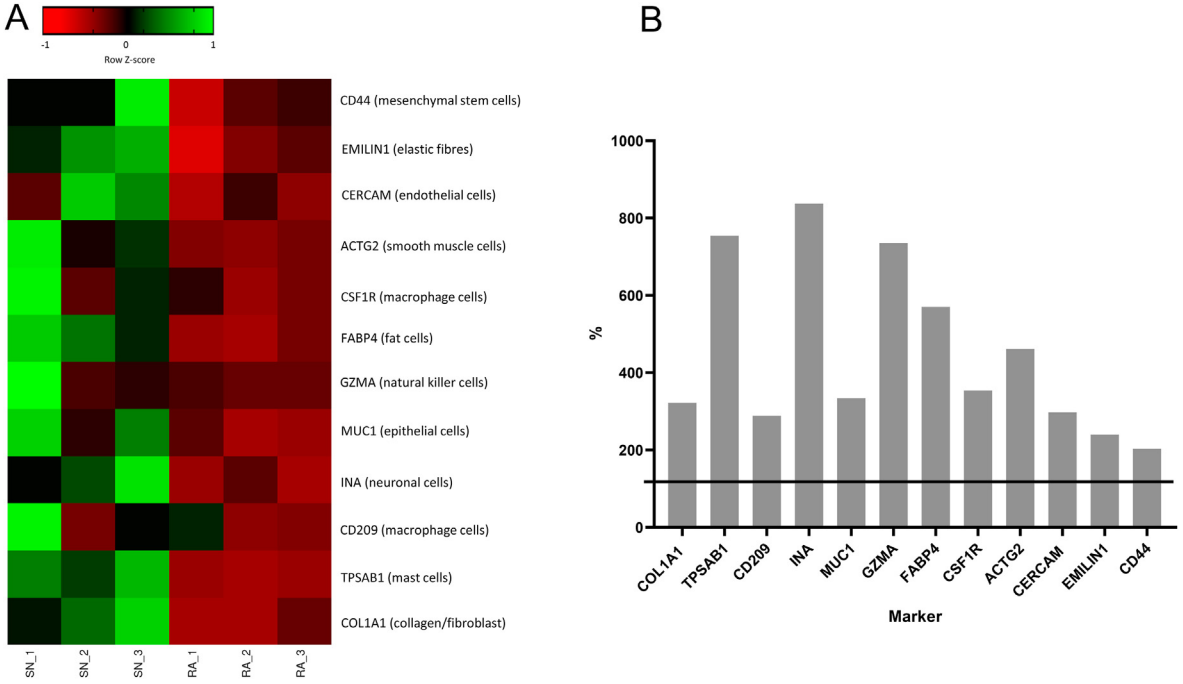

Fig. 6. Expression profile of markers for different cell types in the human adult sinus node vs. right atrial muscle. A, heat map shows inter-individual expression of each marker in each sinus node (SN1 − SN3) and right atrium (RA1 − RA3) samples. **B,** mean expression of cell markers in the sinus node vs. right atrium (n = 3) plotted as % SN/RA (see Table 4 for details). The black line at 100% represents the markers expression in the right atrium (i.e., basal level). SN = sinus node; RA = right atrium.

the immune system) were more highly expressed in the adult human SN (Fig. 7B). Table 4 lists those HLA markers and their mean ± SEM expression profile in 3 SN and 3 RA. Their expression as % SN over RA is also included in Table 4 and shown graphically in Fig. 6B. The heat map shows their expression profile in each sample (Fig. 7A).

The high expression of HLAs together with high expression of macrophages, mast and natural killer cells in the adult human SN is of great interest are may be related to slower heart rates in COVID19 patients (Amaratunga et al., 2020; Capoferri et al., 2020). As already mentioned in the introduction, the importance of macrophages in maintaining HR and rhythm has been explored by (Hulsmans et al., 2017).

Table 4 lists collagen isoforms and their mean ± SEM expression profiles in 3 SN and 3 RA. The heat map shows their expression profile in each sample (Fig. 8A). Their expression as % SN over RA is also included in Table 4 and shown graphically in Fig. 8B. Collagens are linked to cardiac fibrosis (Dobrzynski et al., 2013; Zhang et al., 2000; Wynn 2009). We have identified 11 collagen isoforms that are highly expressed in the SN compared to RA (Fig. 8). Out of the 11-collagen isoforms, COL9A2 (365% SN/RA is most abundant), however, COL9A3, COL8A2 and COL1A1 are also highly abundant in the human adult SN (Fig. 8B).

3.5. Contractile apparatus and related markers and mitochondria markers are less expressed in the adult human SN vs. right atrium

Table 4 lists markers for the contractile apparatus and mitochondria and their mean ± SEM expression profiles in 3 SN and 3 RA. The heat maps show their expression profile in each sample (Figs. 9A and 10A). Their expression as % SN/RA is also included in Table 4 and shown graphically in Figs. 9B and 10B. Each marker is abundantly less in the SN samples compared to the RA (Figs. 9B and 10B).

The SN myocytes are not contractile cells and are known to be 'empty' due to poor expression of the contractile machinery (Choudhury et al. 2015; James et al., 1966; Boyett et al. 2000). All contractile markers: actin (ACTN2), myosin heavy chain 6 (MYH6), titin (TTN), troponin T (TNNT2), as well as, desmin (DES (Yamamoto et al., 2011); and dystrophin (DMD (Williams and Bloch 1999); are less expressed in the human adult SN vs. RA. MYH6, a well-established marker for atrial cells (Gelb and Chin 2012; Ching et al., 2005), is approximately 80% less expressed in the SN/RA (Fig. 10B).

The SN cells also contain less mitochondria (James et al., 1966). We observed that various isoforms of mitochondria (MRPs) are less abundant in the adult human SN compared to RA (Fig. 9B). All of these isoforms were similarly twice less expressed in the SN (around 50%) to that of RA.

We summarised the expression profiles of the markers of cells, collagen, HLA, mitochondria and contractile machinery in the SN according to their log2foldchange to show their clustering (Fig. 11). The markers for the non-cardiac cell types (smooth muscle, macrophage, fat, neuronal, epithelial, mast, endothelial, natural killer, mesenchymal stem cells) are mostly expressed in the SN and they cluster together (Fig. 11). The least expressed markers in the SN also cluster together (Fig. 11).

3.6. Prediction of interactions of novel transcription factors and markers for cell types and contractile machinery

After identifying novel TFs within our dataset and quantification of various cell markers/organelles, we aimed to use IPA to determine if any of the key 'novel' TFs activate/inhibit the key markers specific to the SN. Several cross-control pathways were identified with IPA and are shown in Fig. 12A and B. Both RUNX1 and RUNX3 are activating mast cells; RUNX1 is also activating macrophages along with CEBPA. CEBPA also activates fat cells and RUNX2 activates fibroblasts (Fig. 12A). The TFs, GLI1 activates RUNX2, fibroblasts and CD44 (Fig. 12A). MEFA2A (more expressed in the RA) activates MYH6 (atrial myocyte marker which is more expressed in the RA vs. SN).

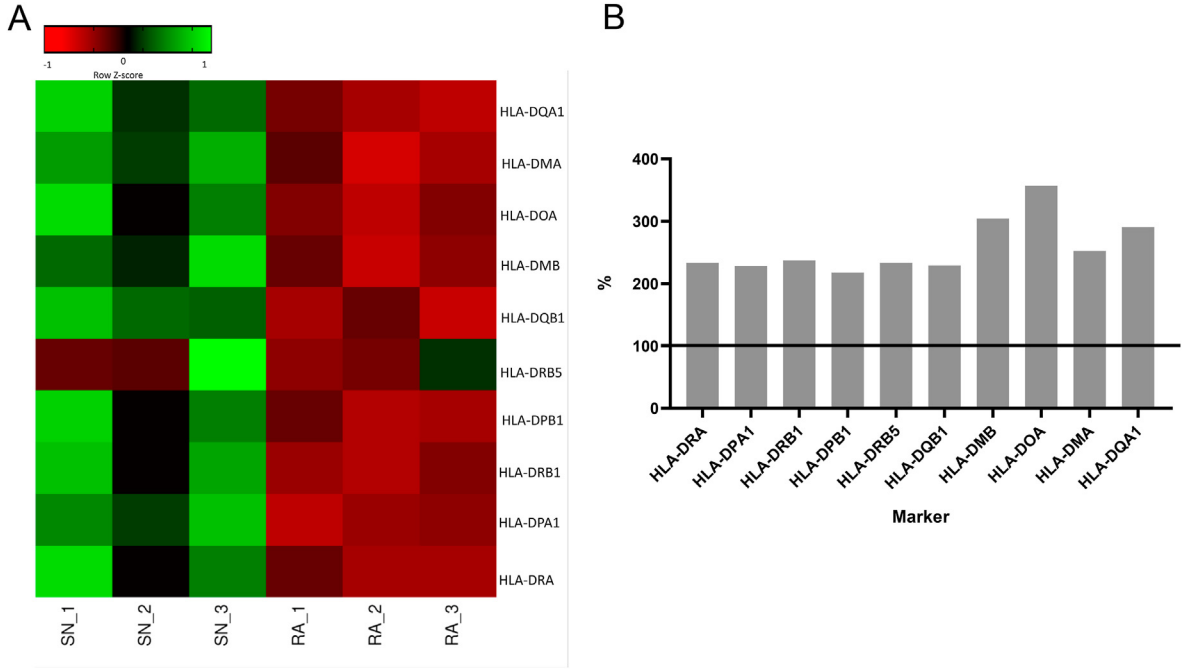

Fig. 7. Expression profile of human leukocyte antigen markers in the human sinus node vs. right atrium. A, heat map shows inter-individual expression of HLA markers in each sinus node (SN1 – SN3) and right atrium (RA1 – RA3) samples. **B,** mean expression in the sinus node vs. right atrium (n = 3) plotted as % SN/RA (see Table 4 for details). The black line at 100% represents HLA expression in the right atrium (i.e., basal level). SN = sinus node; RA = right atrium; HLA = human leukocyte antigen (major histocompatibility complex class I).

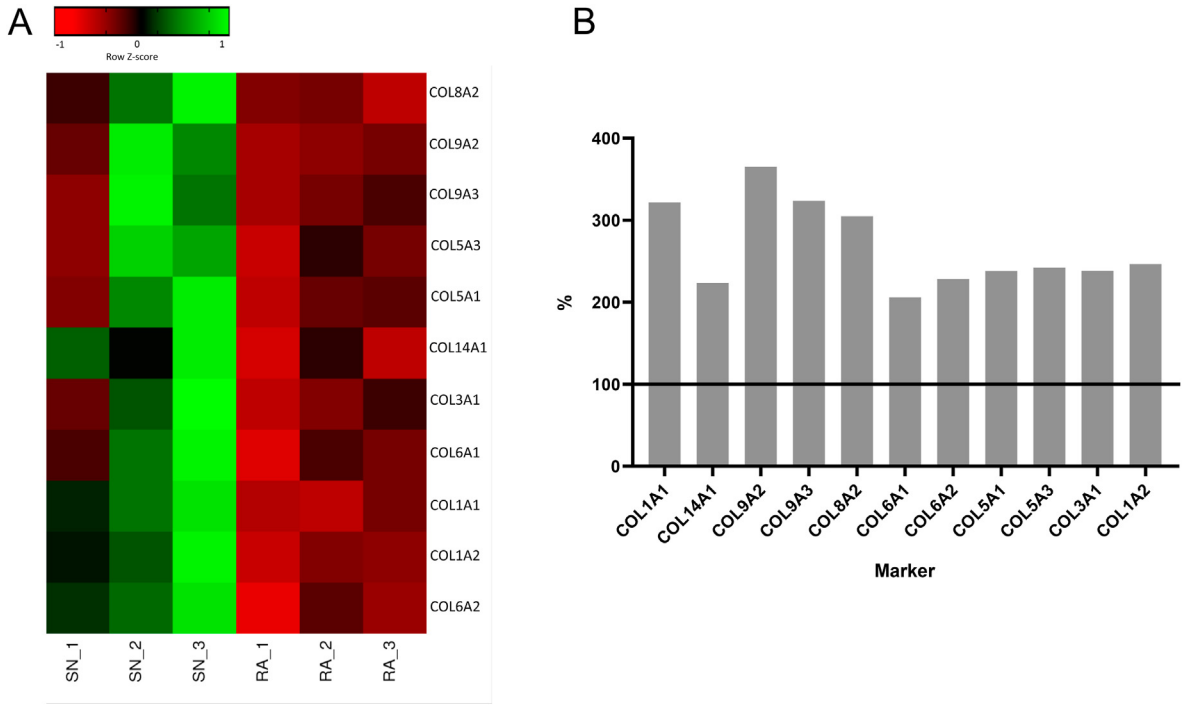

Fig. 8. Expression profile of collagen isoforms expressed in the adult human sinus node vs. right atrial muscle. A, heat map shows inter-individual expression of various collagen markers in each sinus node (SN1 – SN3) and right atrium (RA1 – RA3) samples. **B,** mean expression in the sinus node vs. right atrium (n = 3) plotted as % SN/RA (see Table 4 for details). The black line at 100% represents collagens expression in the right atrium (i.e., basal level). SN = sinus node; RA = right atrium; COL = collagen.

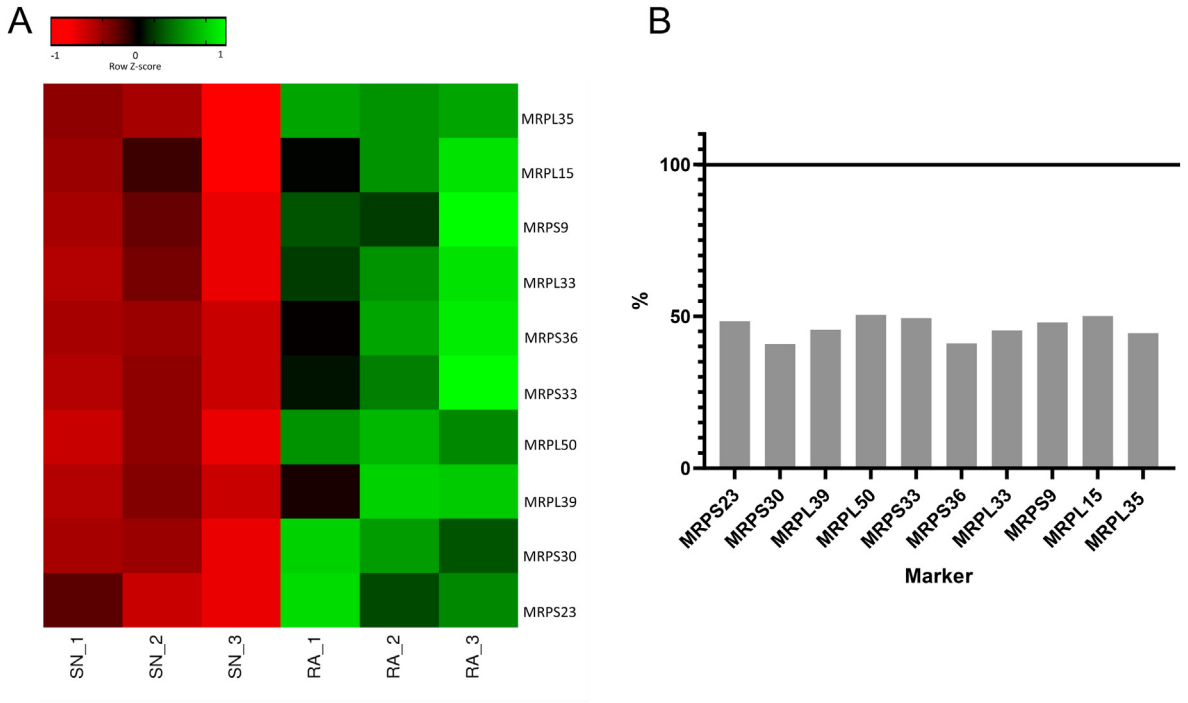

Fig. 9. Expression profile of contractile mitochondria markers in the adult human sinus node vs. right atrial muscle. A, heat map shows inter-individual expression of various mitochondria markers in each sinus node (SN1 – SN3) and right atrium (RA1 – RA3) samples. **B,** mean expression in the sinus node vs. right atrium (n = 3) plotted as % SN/RA (see Table 4 for details). The black line at 100% represents mitochondria markers expression in the right atrium (i.e., basal level). MRP = mitochondrial ribosomal protein; SN = sinus node; RA = right atrium.

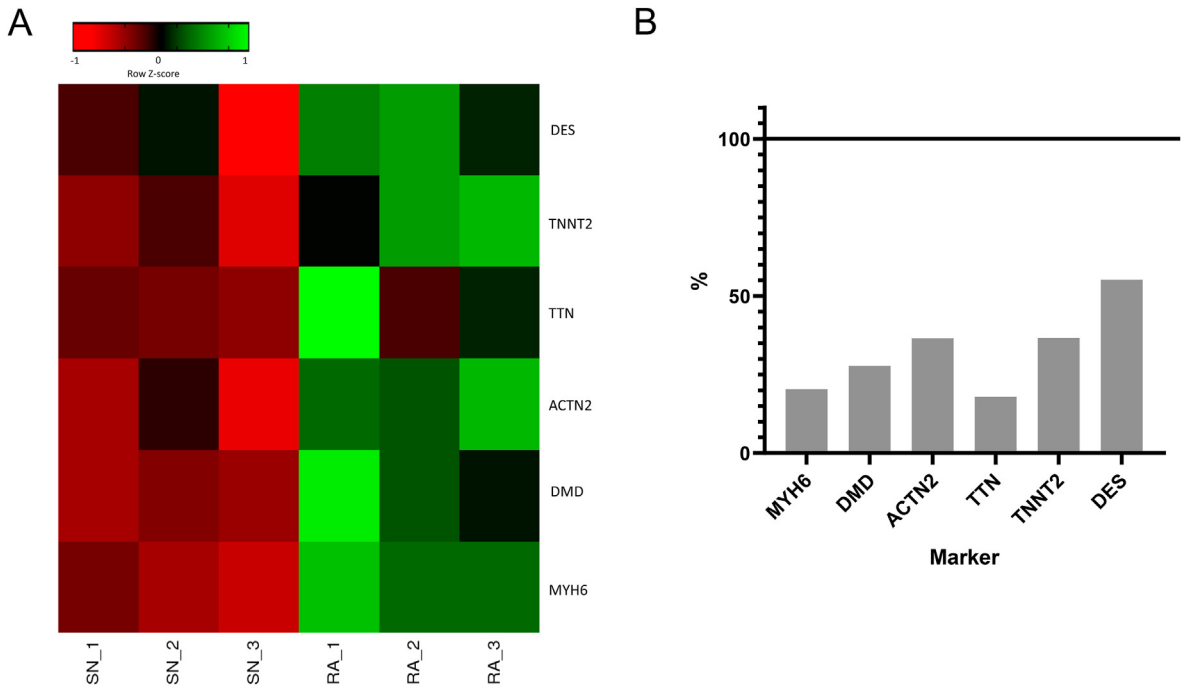

Fig. 10. Expression profile of contractile apparatus/cytoskeletal markers the adult human sinus node vs. right atrial muscle. A, heat map shows inter-individual expression of various contractile/cytoskeletal markers in each sinus node (SN1 – SN3) and right atrium (RA1 – RA3) samples. **B,** mean expression in the sinus node vs. right atrium (n = 3) plotted as % SN/RA (see Table 4 for details). The black line at 100% represents contractile/cytoskeletal markers expression in the right atrium (i.e., basal level). ACTN2 = actinin alpha 2; DES = desmin; DMD = dystrophin; MYH6 = myosin heavy chain 6; RA = right atrium; SN = sinus node; TTN = titin; TNNT2 = troponin T2.

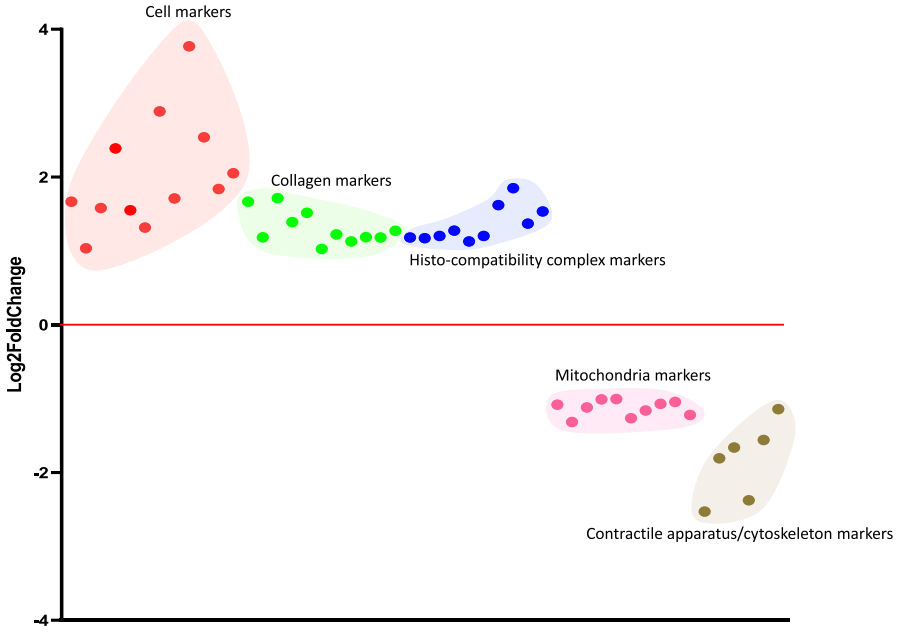

Fig. 11. Summary of expression of all markers as fold change. log2foldchange expression or markers. Log2foldchange>1 = significantly more expressed in the sinus node vs. right atrium; log2foldchange<1 = significantly less expressed in the sinus node vs. right atrium (see Table 4 for details).

3.7. Interaction of key microRNAs with key transcription factors and key cell markers

We have recently published miR profiles of the human adult SN vs. RA (Petkova et al., 2020). We predicted that 15 key miRs are involved in regulation of the two clocks responsible for pacemaking (Petkova et al., 2020). Furthermore, we validated that the funny channel HCN4 is inhibited by miR-486-3p. If miR-486-3p is upregulated that leads to HCN4 downregulation resulting in bradycardia.

Fig. 13 is summarises our key findings on our new predicted interaction. The number of binding sites on the targets interacting with miRs are listed in Table 5. The predicted interactions need to be validated in the future as we did in our recent study by (Petkova

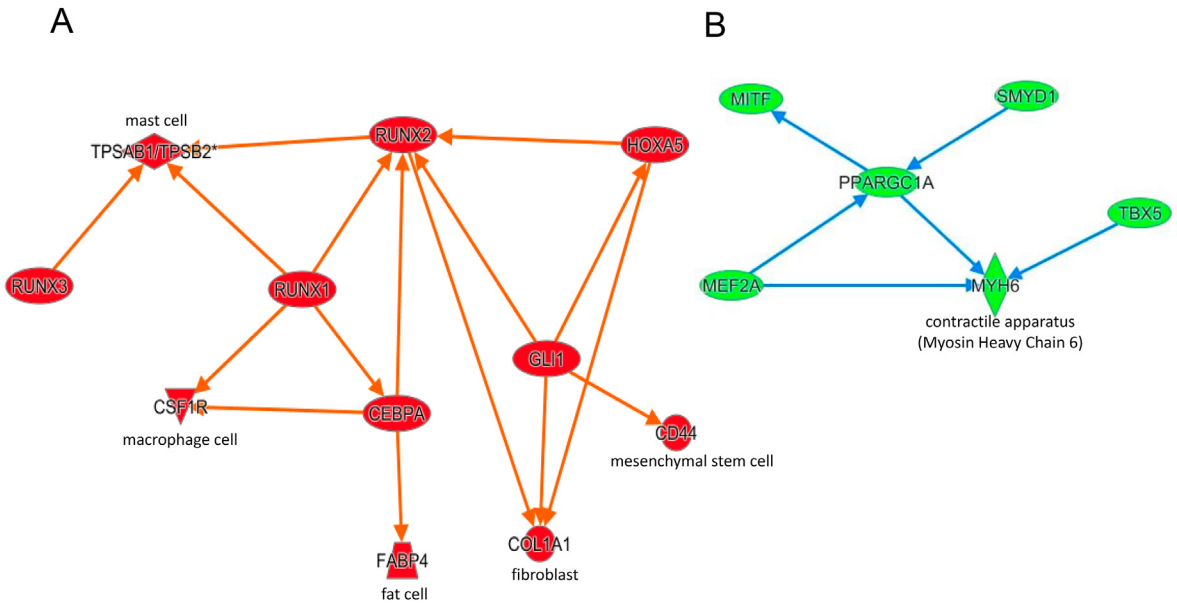

Fig. 12. Ingenuity Pathway Analysis of predicted interactions amongst 'novel' transcription factors and markers. A, transcription factors and markers more abundant in the sinus node vs. right atrium. **B,** transcription factors and markers less abundant in the adult human sinus node vs. right atrium. Arrows = predicted activation; oval shape = transcription factors. Red nodes represent molecules significantly more expressed in the SN. Green nodes represent molecules that are significantly less expressed in the SN (therefore significantly more expressed in the RA).

et al., 2020) for HCN4 and miR-486-3p.

Fig. 13 shows that miR-486-3p interacts with the mast cell marker, TPBAB1, macrophage cell marker, CD209, and other immune system markers (HLAs) as well as endothelial cell marker, CERCAM, (Fig. 13). MiR-133a-3p also inhibits the mast cells and COL1A (Fig. 13). Interestingly, some 'novel' TFs (LZTS1, SOX13, LBH, SOX2, RUNX2 and GLI2), which are highly expressed in the human adult SN are predicted to inhibit those microRNAs that are less expressed in the SN including miR-486-3p, miR-133a-3p, miR-938, miR-429, miR-422a, miR-30c-5p, miR-483-3p (Fig. 13).

It can be suggested that in the SN, RUNX2 activates COL9A3 via inhibition of miR-30c-5p, whereas LZTS1, LBH and SOX13 are activate immune markers via inhibiting miR-486-3p (Fig. 13). It can also be suggested that those miRs that are highly expressed in the SN namely miR-10 b-5p, miR-215-5p miR-1225-3p and miR153-3p inhibit the expression of TBX5, NKX2-5, MITF, MEF2A and PPARGC1A (Fig. 13).

We also hypothesise that increased circulating miR-486-3p in severe COVID-19 patients (Tang et al., 2020) may be responsible for decreased HR (Amaratunga et al., 2020; Capoferri et al., 2020) via inhibition of HCN4 and/or immune markers.

4. Discussion

4.1. The role of 'novel' transcription factors in the sinus node and their predicated interactions with TBX3 and ILS1

In this study we investigated the expression profile of known/'embryonic' and unexplored/'novel' TFs in the human adult SN vs. RA. We explored the interaction pathways of all significantly expressed TFs and their potential role in controlling SN function and structure by interacting with different cell types in this specialised tissue of the heart. Furthermore, we explored the interaction pathways of key miRs with key TFs and markers of different cells.

It is known that TBX3 and ILS1 are important during the embryonic development of the SN (van Eif et al., 2019). These TFs are also expressed in the SN of adult rodent heart (Liang et al., 2015) as well as adult human heart (Petkova et al., 2020; Chandler et al., 2009). Nothing is known about overexpression of these TFs in the adult mammalian SN but TBX3 overexpression in the ventricles of adult mice can induce pacemaker characteristics (Bakker et al., 2012).

Many other 'novel' TFs present in the adult human SN are predicted to interact with TBX3 and ISL1 to regulate the expression of the funny channel, HCN4, (Fig. 5A). It is well known that HCN4 downregulation is responsible for SND and its upregulation can promote atrial arrhythmias (Zicha et al., 2005). ISL1 (the most abundant TF in the human adult SN; Figs. 2 and 3, Table 1), if mutated, can cause sinus bradycardia and sinus arrhythmia (Tessadori et al., 2012; Hoffmann et al., 2013).

As can be seen in Fig. 5A, some 'novel' TFs namely RUNX2 directly activates ISL1 whereas SOX2 activates TBX3 (Fig. 5A). It can therefore be hypothesised that changes to RUNX2 or SOX2 expression (the direct activators of ILS1 and TBX3 respectively; Fig. 5) could also result in SND. RUNX2 (an osteogenic TF) has been detected in the heart, where its overexpression caused significantly lower heart rate in mice (Nakayama et al., 2018). This could be mediated via ISL1 (Fig. 5) or immune cells (Fig. 12) discussed later. SOX2 (one of the most highly expressed TFs in the SN vs. RA; Figs. 2A and 3B, Table 2) is reported to be important for hiPSC generation into diverse cardiac cells from human fibroblasts, which are then further differentiated into pacemaker cells (Schweizer et al., 2017). It has also been reported that overexpression of SOX2 can increase number of differentiated myocytes in mice (Koyanagi et al., 2010).

The precise role of RUNX2 and SOX2 in the SN is not yet understood but their higher expression in the SN and predicted direct interactions with ISL1 and TBX3 can help to maintain the SN structure and function.

Other 'novel' TFs activate ISL1 via RUNX2 to activate HCN4 (Fig. 5A) and GLI1 via SOX2 activates TBX3 to also activate HCN4. Of interest are the following 'novel' TFs: 1). GLI1 (known to be upregulated in diseased mouse heart and is involved in the hedgehog pathway (Xiao et al., 2012); 2). GLI2 is also involved in signalling

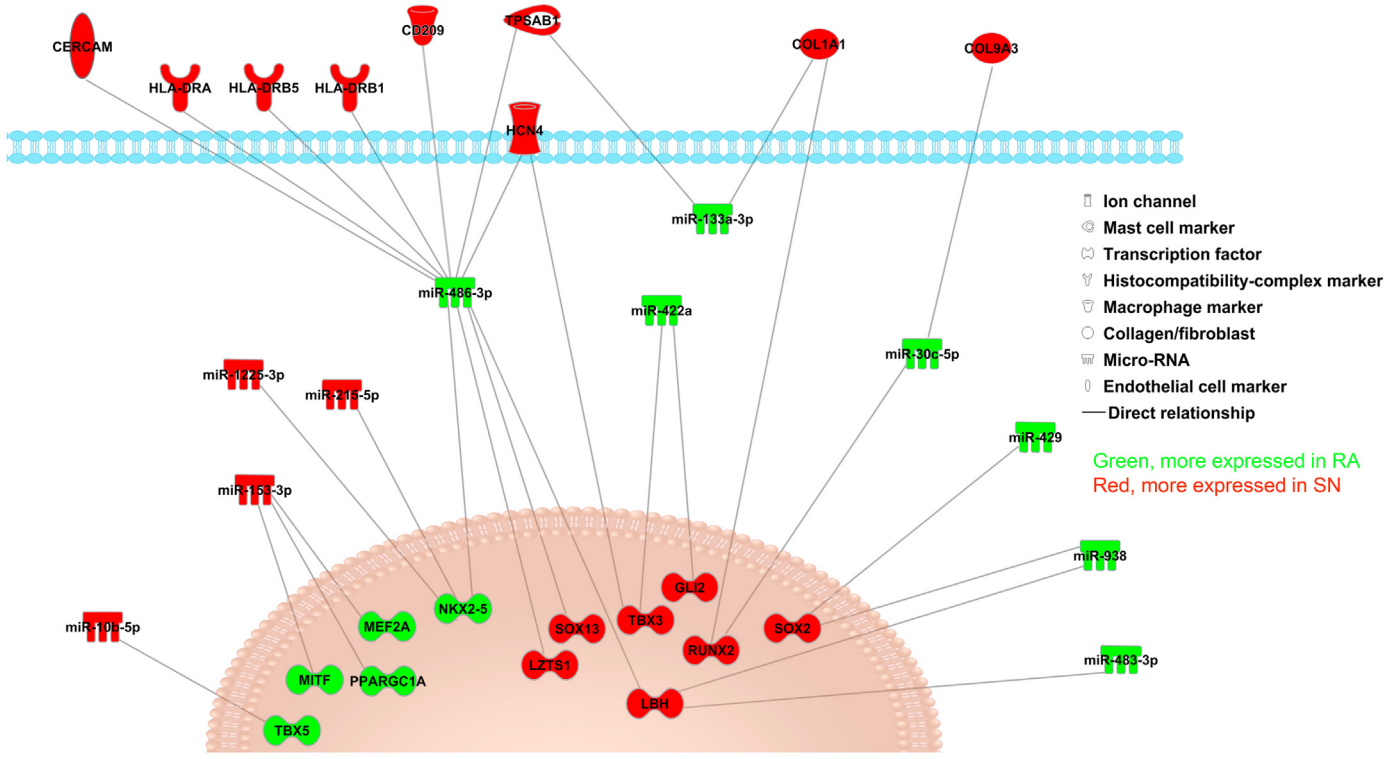

Fig. 13. Ingenuity Pathway Analysis predicted interactions amongst microRNAs, 'novel' transcription factors and markers. Markers are represented by different shapes. Mast cell marker (TPSAB1), macrophage cell marker (CD209), endothelial cell marker (CERCAM), collagen markers (CLO1A1, COL9A3), human leukocyte antigen markers (HLAs) are within ECM. HCN4, funny channel is within the plasma membrane. miRs are in the cytoplasm and transcription factors are shown in the nucleus. Red = more expressed in the SN vs. RA; green = more expressed in the RA vs. SN. ECM = extracellular matrix; miR = microRNAs.

pathways in the heart (Qin et al., 2019); 3). RUNX1 if lost in zebrafish enhances heart regeneration (Koth et al., 2020). Interestingly, ISL1, RUNX2 and TBX3 are also known to be involved in this Sonic hedgehog pathway (Lin et al., 2006; Dunaeva and Waltenberger 2017; Ludtke et al., 2016). TBX3 expression in mouse lungs depends on Sonic hedgehog signalling (Ludtke et al., 2016). RUNX1 depletion results in an altered expression of ISL1 in cancer research (van der Deen et al., 2012).

The 'novel' aforementioned TFs together with TBX3 and ILS1 may help with biological pacemaker formation strategies, human embryonic stem cell differentiation and use as novel therapeutic targets in regenerative medicine.

The role of 'novel' transcription factors in the sinus node and their predicated interactions with markers of immune, fat and fibroblast cells.

Interestingly some of these novel TFs e.g., RUNX1, RUNX2, RUNX3 and CEBPA also activate immune cells (Fig. 12A). This information may be of importance and may suggest that there might be an interaction between immune and nodal cells because both cells types are predicted to be activated by the TFs involved in the same signalling pathways.

We found that the markers for macrophages (CSF1R/CD209, Fig. 6) and the major histocompatibility complex (MHC) components (Fig. 7) are more expressed in the adult human SN compared to RA. Macrophages not only clear foreign antigens and cellular debris but also they are involved in the regeneration of the damaged myocardium through their interaction with other cardiac cells (Pinto et al. 2014). The HLA (human leukocyte antigen) complex is a group of related proteins that are encoded by the MHC and they are cell-surface proteins involved in the regulation of the immune system and are well known as transplantation antigens (Choo 2007). It is well known that CSF1R is important for macrophage development, growth and survival by CEBPA (Zriwil et al., 2016) and RUNX1 (Himes et al., 2005). RUNX3 was also shown to be an important mediator of immune cell development and maturation (Boto et al. 2018).

At gestation, immune cells are recruited into the heart and remain there for life; therefore the immune system is essential for the development and maintenance of the heart. In response to infection or after myocardial infraction, immune cells are essential for repairing the damaged tissue (Swirski and Nahendorf 2018). In the mouse AV node a high expression of macrophages was discovered by (Hulsmans et al., 2017) that are electrically coupled with AV node cells via Cx43. The depletion of macrophages in mice results in AV block and lower heart rate (Hulsmans et al., 2017). This research group also noticed that HCN4-expressing cardiomyocytes in the AV node frequently scattered with macrophages (Hulsmans et al., 2017).

It is likely that the depletion of immune cells in diseased SN can cause lower heart rate via Cx45 dysregulation (the main gap junction channel in the human SN; Chandler et al., 2009).

RUNX2, GLI1 and HOXA5 activate fibroblasts, CEBPA activates fat cells and GLI1 also activates mesenchymal stem cells (Fig. 12A). We have previously shown that there is an increase in connective tissue (mainly collagen content - an indicator of fibrosis) as well as fat in the aged cardiac conduction system (Kharche et al., 2017; Saeed et al., 2018; Csepe et al., 2015). Ageing is a risk factor of SND, and increased fibrosis is observed in sick sinus syndrome (Csepe et al., 2015). When activated fibroblasts secrete excessive extracellular matrix, which can lead to pathological fibrosis and organ failure (Zhang et al., 2019). In our current study, we observed a high expression profile of 11 different isoforms of collagens (Fig. 8A) and FABP4 (a fat cell marker - Fig. 6B) in the adult human SN. Highly expressed collagen 1A1 is predicted to be activated by RUNX2, GLI1

and HOXA5. HOXA5 is known to be expressed in fibroblasts and its upregulation depends on GLI1-dependent Hedgehog signalling (Zhang et al., 2019; Katoh and Katoh 2005) and RUNX2 has also been shown to be involved in fibrosis (Hsu et al., 2017).

An increase in fat content can also contribute to SND (Shiraishi et al., 1992), therefore it would be interesting to know if CEBPA and FABP4 are also increased in the diseased SN. It has recently been reported that they are involved in adipogenesis and FABP4 is expressed in the mature fat cells (Bahrami-Nejad et al., 2020).

Collectively our data suggests that similar TFs are involved in regulation of different cell types in the SN (namely immune, nodal, fat and fibroblasts) in health. RUNX1 is of particular interest because it not only regulates key TFs involved in the regulation of primary pacemaker cell (Fig. 5) activity but are also involved in regulation of other cell types present in the SN (Fig. 12) and perhaps can offer new treatment for SND. In fact, RUNX1 has recently been reported to offer a new emerging target for treatment for cardiovascular diseases (Riddell et al., 2020).

The SN is non-contractile tissue and has fewer myofilaments and fewer mitochondria than in RA (Bleeker et al., 1980; Marvin et al., 1984; Boyett et al. 2000; Christoffels et al., 2010). Therefore, as expected, there is a lower expression of contractile machinery and mitochondria in the adult human SN compared to the RA (Figs. 9 and 10). TFs, MEFA2A, TBX5 and NKX2-5 are activating Ca^{2+} handing proteins in the RA (Fig. 5B), which are less expressed in the SN (Chandler et al., 2009). It is reported that the knock-out of NKX2-5 in mouse heart resulted in the repression of RYR2 (Briggs et al., 2008). Interestingly MEF2A (known to regulate structural proteins – (Guo et al., 2014)), together with TBX5 activates MYH6 (involved in the contractile machinery in the working atrial muscle) (Fig. 12B).

4.2. The role of microRNAs in the sinus node and their predicted interactions with transcription factors and other markers

Interestingly, Fig. 13 shows that lower expression of MEF2A and NKX2-5 in the SN may be due to higher expression of miR-153-3p and miR-1225-3p, which are also predicted to inhibit RYR2 and $Na_v1.5$ respectively which are less expressed in the SN (Petkova et al., 2020; Chandler et al., 2009).

The 'novel' TFs namely: SOX2, RUNX2 and LBH inhibit the expression of e.g., miR-30c-5p, miR-938 in the SN hence explain the higher expression of $Ca_v1.3$ (Petkova et al., 2020; Chandler et al., 2009) and COL9A3 (Fig. 13).

The TFs LZTS1, SOX13 and LBH, which are highly expressed in the adult human SN vs. RA, and are predicted to inhibit miR-486-3p, which can explain higher expression of HCN4 and immune markers in the SN vs. RA (Fig. 13). LZTS1 has as many as 12 binding sites for miR-486-3p (Table 5); therefore it is also possible that miR-486-3p is inhibiting LZTS1 expression in the RA. LZTS1 is a TF that plays a role in the regulation of cell growth and proliferation and deficiency of this TF is reported to cause cancer in human cell lines (Cabeza-Arvelaiz et al., 2001).

It has already been mentioned that sinus bradycardia in COVID-19 patients has recently been reported by (Amaratunga et al., 2020; Capoferri et al., 2020), which has been postulated to be caused by hypoxia and inflammatory damage of the SN cells. It has also been recently reported that circulating miR-486-3p is upregulated in COVID-19 patients, which may result in immune response dysregulation (Tang et al., 2020). It is possible that upregulation of miR-486-3p can cause changes in the connective tissue flora via mast and macrophage cells and HLAs dependent pathological conditions in the SN in addition to the direct HCN4 suppression leading to sinus bradycardia (Fig. 13). Furthermore, SND can also be attributed to changes in immune response and fibrosis via changes in miR-133a-3p and RUNX2 (Fig. 13).

The interactions of miR-486-3p and miR-133a-3p with immune and/or fibroblast markers and 'novel' TFs (Fig. 13) requires further validation.

All this puzzling information on the high expression of immune markers' in the SN vs. RA and their complex interactions with TFs and miRs leads to the question "why does the SN require such high expression of immune response markers"? (Hulsmans et al., 2017) showed that macrophages are involved in healthy functioning of the mouse AV node. Here we report that the immune system is likely to be important for the maintenance of a healthy functioning human SN. The high expression of innate immune system natural killer cells, macrophages and HLAs (present on the surface of most cells) in the SN may play an important role in the immune response to foreign material (Fig. 13). It is possible that this high expression of HLAs, natural killer and macrophage cells rapidly respond to virus infections and other pathological stimuli in the SN may cause an obstacle for the development of biological pacemakers (Hu et al., 2014; Kapoor et al., 2013; Kapoor et al. 2011). The development and delivery of TFs and/or miRNAs as biological pacemakers is a difficult task, primarily due to the fact that the SN induces a rapid immune response against foreign matter. Hu et al. studied the adenoviral vector-delivery of TBX18 (expressed in the adult human SN (Petkova et al., 2020);) in a swine model of total heart block where the pacemaking activity was stabilised but after day 7 the heart rate started to decrease due to an immune response by the host tissue (Hu et al., 2014). Thus our results and the studies carried out by other groups confirm significance of the immune system cells in the SN functioning.

5. Conclusion

The morphology and mechanisms of the adult human SN are incredibly complex. There is a unique expression of 'novel' TFs in the adult human SN tissue that most likely work together with TBX3 and ISL1 to regulate the expression of the funny channel as well as immune cells in health and could contribute to SND. Our study provides novel insights into the complex underlying mechanisms that control molecular, morphological and functional characteristics of the tissue that makes our heartbeat. It also provides novel perception into the importance of the immune response that contributes to functioning of the primary pacemaker of the heart. In an increasing global ageing population, the occurrence of SND is increasing, therefore key 'novel' TFs, immune marker cells and miRs identified in this study should be explored for functional validation and for potential therapeutic management of SND.

Authors' statement/contribution

Abimbola J Aminu (AJA): contributed to planning and manuscript writing, analysis of NGS data, bioinformatics, histology; creating all figures and tables; discussed with HD on format of manuscript and figures. Maria Petkova (MP): contributed to cryosectioning, histology, RNA extraction, NGS analysis and bioinformatics. Andrew J Atkinson (AJA): contributed to RNA extraction, cryosectioning, histology and supervision of MP, ADM, RTS. Joseph Yanni (JY): contributed to RNA extraction and supervision of MP. Alex D Morris (ADM): contributed to cryosectioning and histology. Robert T Simms (RTS): contributed to NGS analysis and bioinformatics. Weixuan Chen (WC): contributed to morphological and NGS analysis and bioinformatics. Zeyuan Yin (ZY): contributed to NGS analysis and bioinformatics. Mateusz K. Holda (MKH): provided comments on the manuscript. Marcin Kuniewicz MP): provided interesting ideas related to revision of the manuscript.

Vladislav S. Kuzmin (VSK): contributed to editing and writing manuscript. Filip Perde (FP): provided human specimens. Peter Molenaar (PM): provided human specimens, edited the manuscript and provided comments on Figuers and Tables. Halina Dobrzynski (HD): conceived research, obtained funding, supervised AJA, MP, ADM, RTS, WC, ZY, contributed to planning and writing of manuscript, analysis of data, formatting figures and tables. All authors approved the manuscript.

Source of funding

This work was supported by the British Heart Foundation program grant FS/17/67/33,483 and the Leducq Foundation (THE FANTACY 19CVD03).

Disclosures

None.

Declaration of competing interest

The authors declare no conflict of interest.

Acknowledgment

We would like to thank Ian Donaldson for his help with NGS analysis and plotting volcano plots.

References

Alboni, P., Filippi, L., Pirani, R., De Lorenzi, E., Masoni, A., 2007. The role of the autonomic nervous system on sinus node function in patients with intermittent sinoatrial block. J. Electrocardiol. 17, 25–32.
Alfieri, C.M., Cheek, J., Chakraborty, S., Yutzey, K.E., 2010. Wnt signalling in the heart development and osteogenic gane induction. Dev. Biol. 338, 127–135.
Amaratunga, E.A., Corwin, S.D., Moran, L., Snyder, R., 2020. Bradycardia in patients with COVID-19: a calm before the storm? Cureus 12, e8599.
Bahrami-Nejad, Z., Chen, T., Tholen, S., Rabiee, A., Zhao, M.L., Bielczyk-Macynzka, E., Braemer, F.B., Teruel, M.N., 2020. The Highly Expressed Lipid Buffer FABP4 Enforces Adipocyte Cell Identity by Driving the Initial Cell Differentiation Process.
Bakker, M.L., Boink, J.J.G., Boukens, J.B., Verkerk, O.A., van den Boogaard, M., den Haan, D.A., Hoogaars, H.M.W., p Buermans, H., 2012. T-box transcription factor TBX3 reprogrammes mature cardiac myocytes into pacemaker-like cells. Cardiovasc. Res. 94, 439–449.
Baum, P.D., Garriga, G., 1997. Neuronal migrations and axon fasciculation are disrupted in ina-1 integrin mutants. Neuron 19, 51–62.
Bleeker, W.K., Mackaay, A.J., Masson-Pevet, M., Jongsma, H.J., Bouman, L.N., Becker, A.E., 1980. Functional and morphological organization of the rabbit sinus node. Circ. Res. 46, 11–22.
Bode, M., Wu, Y., Pi, X., Lockyer, P., Dechyapirom, W., Portbury, A.L., Patterson, C., 2011. Regulation of ASB4 expression in the immortalized murine endothelial cell lines MS1 and SVR: a role for TNF- α and oxygen. Cell Biochem. Funct. 29, 334–341.
Boto, P., Csuth, T.I., Szatmari, I., 2018. Runx3-mediated immune cell development and maturation. Crit. Rev. Immunol. 38, 63–78.
Boyett, M.R., Honjo, H., Kodama, I., 2000. The sinoatrial node, a heterogeneous pacemaker structure. Cardiovasc. Res. 47, 658–687.
Briggs, E.L., Takeda, M., Cuadra, E.A., Wakimoto, H., Marks, H.M., Walker, J.A., Seki, T., Oh, P.S., Lu, T.J., Summers, C., Raizada, K.M., Horikoshi, N., Weinberg, O.E., Yasui, K., Ikeda, Y., Chien, R.K., Kasahara, H., 2008. Perinatal loss of Nkx2-5 results in rapid conduction and contraction defects. Circ. Res. 103, 580–590.
Brown, H.F., Difrancesco, D., Noble, S.J., 1979. How does adrenaline accelerate the heart? Nature 280, 235–236.
Cabeza-Arvelaiz, Y., Sepulveda, J.L., Lebovitz, R.M., Thompson, T.C., Chinault, C.A., 2001. Functional identification of LZTS1 as a candidate prostate tumor suppressor gene on human chromosome 8p22. Oncogene 20, 4169–4179.
Callis, E.T., Wang, D.-Z., 2008. Taking microRNAs to heart. Trends Mol. Med. 14, 254–260.
Capoferri, G., Oshoff, M., Egli, A., Stoeckle, M., Bassetti, S., 2020. Relative Bradycardia in Patients with COVID-19. CMI.
Chandler, J.N., Greener, D.I., Tellez, O.J., Inada, S., Musa, H., Molenaar, P., DiFrancesco, D., Baruscotti, M., Longhi, R., Anderson, H.R., Billeter, R., Sharma, V., Sigg, C.D., Boyett, R.M., Dobrzynski, H., 2009. Molecular architecture of the human sinus node insights into the function of the cardiac pacemaker. Circulation 119, 1562–1575.
Chandler, N., Aslanidi, O., Buckley, D., Inada, S., Birchall, S., Atkinson, A., Kirk, D., Monfredi, O., Molenaar, P., Anderson, R., Sharma, V., Sigg, D., Zhang, H., Boyett, M., Dobrzynski, H., 2011. Computer three-dimensional anatomical reconstruction of the human sinus node and a novel paranodal area. Anat. Rec. 294, 970–979.
Ching, Y.H., Ghosh, T.K., Cross, S.J., Packham, E.A., Honeyman, L., Loughna, S., Robinson, T.E., Dearlove, A.M., Ribas, G., Bonser, A.J., Thomas, N.R., Scotter, A.J., Caves, L.S.D., Tyrrell, G.P., Newbury-Ecob, R.A., Munnich, A., Bonnet, D., Brook, D.J., 2005. Mutation in myosin heavy chain 6 causes atrial septal defect. Nat. Genet. 37, 423–428.
Choo, S.Y., 2007. The HLA system: genetics, immunology, clinical testing, and clinical implications. Yonsei Med. J. 48, 11–23.
Choudhury, M., Boyett, R.M., Morris, M.G., 2015. Biology of the sinus node and its disease. Arrhythmia Electrophysiol. Rev. 4, 28–34.
Christoffels, V.M., Smits, G.J., Kispert, A., Moorman, A.F.M., 2010. Development of the pacemaker tissues of the heart. Circ. Res. 106, 240–254.
Csepe, T.A., Kalyanasundaram, A., Hansen, B.J., Zhao, J., Federov, V.V., 2015. Fibrosis: a structural modulator of sinoatrial node physiology and dysfunction. Front. Physiol. 6, 37.
Cursons, J., Souze-Fonseca-Guimaraes, F., Foroutan, M., Anderson, A., Hollande, F., Hediyeh-Zadeh, S., Behren, A., Huntington, D., Davis, M.J., 2019. A gene signature predicting natural killer cell infiltration and improved survival in melanoma patients. Cancer Immunol Res 7, 1162–1174.
Desjardins, C.A., Naya, F.J., 2016. The function of the MEF2 family of transcription factors in cardiac development, cardiogenomics, and direct reprogramming. J Cardiovasc Dev Dis 3, 26.
Dhar, P., McAuley, J., 2019. The role of the cell surface mucin MUC1 as a barrier to infection and regulator of inflammation. Front. Cell Infect. Microbiol. 9, 117.
DiFrancesco, D., 2020. A brief history of pacemaking. Front. Physiol. 10, 1599.
Dobrzynski, H., Anderson, H.R., Atkinson, A., Borbas, Z., D'Souza, A., Fraser, F.J., Inada, S., Logantha, J.R.J.S., Monfredi, O., Morris, M.G., Moorman, M.F.A., Nikolaidou, T., Schneider, H., Szuts, V., Temple, P.I., Yanni, J., Boyett, R.M., 2013. Structure, function and clinical relevance of the cardiac conduction system, including the atrioventricular ring and outflow tract tissues. Pharmacol. Therapeut. 139, 260–288.
Dunaeva, M., Waltenberger, J., 2017. Hh signaling in regeneration of the ischemic heart. Cell. Mol. Life Sci. 74, 3481–3490.
Duncan, J.G., Finck, B.N., 2007. The PPAR α -PGC-1 α axis Controls Cardiac Energy Metabolism in Healthy and Diseased Myocardium. PPAR Research, pp. 1–10, 2008.
Friedman, C.E., Nguyen, Q., Lukowski, S.W., Helfer, A., Chiu, H.S., Miklas, J., Levy, S., Suo, S., Han, J.-D., , J., Osteil, P., Peng, G., Jing, N., Baillie, G.J., Senabouth, A., Christ, A.N., Bruxner, T.J., Murry, C.E., Wong, E.S., Ding, J., Wang, Y., Hudson, J., Ruohola-Baker, H., Bar-Joseph, Z., Tam, P.P.L., Powell, J.E., Palpant, N.J., 2018. Single-cell transcriptome analysis of cardiac differentiation from human PSCs reveals HOPX-dependent cardiomyocyte maturation. Cell Stem Cell 23, 586–598.
Fu, Y., Chang, A.C.Y., Fournier, M., CHnag, L., Niessen, K., Karsan, A., 2011. RUNX3 maintains the mesenchymal phenotype after termination of the Notch signal. J. Biol. Chem. 286, 11803–11813.
Gelb, B.D., Chin, S.E., 2012. Genetics of congenital heart disease. Muscle. Academic Press.
Guo, Y., Kuhl, S.J., Pfitser, A.S., Cizelsky, W., Denk, S., Beer-Molz, L., Kuhl, M., 2014. Comparative analysis reveals distinct and overlapping functions of Mef2c and Mef2d during cardiogenesis in Xenopus larvis. PloS One 9, e83294.
Himes, S.R., Cronau, S., Mulford, C., Hume, D.A., 2005. The Runx1 transcription factor controls CSF-1-dependent and -independent growth and survival of macrophages. Oncogene 24, 5278–5286.
Hoffmann, S., Berger, I.M., Glaser, A., Bacon, C., Li, L., Gretz, N., Steinbeisser, H., Rottbauer, W., Just, S., Rappold, G., 2013. Islet1 is a direct transcriptional target of the homeodomain transcription factor Shox2 and rescues the Shox2-mediated bradycardia. Basic Res. Cardiol. 108, 339.
Hoogaars, W.M.H., Engel, A., Brons, J.F., Verkerk, A.O., de Lange, F.J., Wong, L.Y.E., Bakker, M.L., Clout, D.E., Wakker, V., Barnett, P., Ravesloot, J.H., Moorman, A.F.M., Verheijck, E.E., Christoffels, V.M., 2007. Tbx3 controls the sinoatrial node gene program and imposes pacemaker function on the atria. Genes Dev. 21, 1098–1112.
Hsu, C.-K., Lin, H.-H., Harn, H.I., Ogawa, R., Wang, Y.-K., Ho, Y.-T., Chen, W.-R., Lee, Y.-C., Lee, J.Y.-Y., Shieh, S.-J., Cheng, C.-M., MGrath, J.A., Tang, M.-J., 2017. Caveolin-1 controls hyperresponsiveness to mechanical stimuli and fibrogenesis-associated Runx2 activation in keloid fibroblasts. J. Invest. Dermatol. 138, 208–218.
Hu, Y.F., Dawkins, H.C., Cho, E., Marban, E., Cingolani, E., 2014. Biological pacemaker created by minimally invasive somatic reprogramming in pigs with complete heart block. Sci. Transl. Med. 6, 254ra94.
Hu, Y., Li, N., Liu, L., Zhang, H., Xue, X., Shao, X., Zhang, Y., Lang, X., 2019. Genetically modified porcine mesenchymal stem cells by lentiviral tbx18 create a biological pacemaker. Stem Cell. Int. 7, 3621314.
Hulsmans, M., Clauss, S., Xiao, Aguirre, D.A., King, R.K., Hanley, A., Hucker, J.W., Wulfers, M.E., Seemann, G., Courties, G., Iwamoto, Y., Sun, Y., Savol, J.A., Sager, B.H., Lavine, J.K., Fishbein, A.G., Capen, E.D., Da Silva, N., Miquerol, L., Wakimoto, H., Seidman, E.C., Seidman, G.J., Sadreyev, I.R., Naxerova, K., Mitchell, N.R., Brown, D., Libby, P., Weissleder, R., Swirski, K.F., Kohl, P., Vinegoni, C., Milan, J.D., Ellinor, T.P., Nahrendorf, M., 2017. Macrophages

facilitate electrical conduction in the heart. Cell 169, 510–522.
James, T.N., Sherf, L., Fine, G., Morales, A.R., 1966. Comparative ultrastructure of the sinus node in man and dog. Circulation 34, 139–163.
Kapoor, N., Liang, W., Marban, E., Cho, H.C., 2013. Direct conversion of quiescent cardiomyocytes to pacemaker cells by expression of Tbx18'. Nat. Biotechnol. 31, 54–62.
Kapoor, N., Marban, E., Cho, H.C., 2011. Biological pacemaker induced in vivo by focal Tbx18 gene transfer in the Guinea-pig left ventricle. Circulation 124, A15845.
Katoh, Y., Katoh, M., 2005. Hedhehog signaling pathway and gastric cancer. Canc. Biol. Ther. 4, 1050–1054.
Keith, A., Flack, M., 1907. The form and nature of the muscular connections between the primary divisions of the vertebrate heart. J Anat Physiol 41, 172–189.
Kharche, R.S., Vigmond, E., Efimov, R.I., Dobrzynski, H., 2017. Computational assessment of the functional role of sinoatrial node exit pathways in the human heart. PloS One 12, e0183727.
Koth, J., Wang, X., Killen, A.C., Stockdale, W.T., Potts, H.G., Jefferson, A., Bonkhofer, F., Riley, P.R., Patient, K.R., Gottgens, B., Mommersteeg, M.T., 2020. Runx1 promotes scar deposition and inhibits myocardial proliferation and survival during zebrafish heart regeneration. Development 147, dev186569.
Koyanagi, M., Iwasaki, M., Rupp, S., Tedesco, S.F., Yoon, C.-H., Boeckel, J.-N., Trauth, J., Schutz, C., Ohtani, K., Goetz, R., Lekushi, K., Bushoven, P., Momma, S., Mummery, C., Passier, R., Henschler, R., Akintuerk, H., Schranz, D., Urbich, C., Galvez, G.B., Cossu, G., Zeiher, A., Dimmeler, S., 2010. Sox2 transduction enhances cardiovascular repair capacity of blood-derived mesoangioblasts. Circ. Res. 106, 1290–1302.
Leitoguinho, A.R., Ng, E., Stanley, E., Elefanty, A., 2019. The role of ventx homeobox gene during human haematopoietic development. Exp. Hematol. 76, S73.
Lescroart, F., Zaffran, S., 2018. Hox and Tale transcription factors in heart development and disease. Int. J. Dev. Biol. 62, 11–12.
Liang, X., Zhang, Q., Cattaneo, P., Zhuang, S., ong, X., Spann, N.J., Jiang, C., Cao, X., Zhao, X., Zhang, X., Bu, L., Wang, G., Chen, H.S., Zhaung, T., Yan, J., Geng, P., Luo, L., Banerjee, I., Chen, Y., Glass, C.K., Zambon, A.C., Chen, J., Sun, Y., Evans, S.M., 2015. Transcription factor ISL1 is essential for pacemaker development and function. J. Clin. Invest. 125, 3256–3268.
Lin, L., Bu, L., Cai, C.-L., Zhang, X., Evans, S., 2006. Isl1 is upstream of sonic hedgehog in a pathway required for cardiac morphogenesis. Dev. Biol. 295, 756–763.
Lombardo, R.C., Porollo, A., Cnota, J.F., Hopkin, R.J., 2018. Cogenital heart disease and aortic arch variants associated with mutation in PHOX2B. Genet. Med. 20, 1538–1543.
Ludtke, T.H., Rudat, C., Wojahn, I., Weiss, A.-C., Kleppa, M.-J., Kurz, J., Farin, H., Moon, A., Christoffels, V.M., Kispert, A., 2016. Tbx2 and Tbx3 act downstream of Shh to maintain canonical Wnt signalling during branching morphogenesis of the murine lung. Dev. Cell 39, 239–253.
Lyons, J.J., Yu, X., Hughes, J.D., Le, Q.T., Jamil, A., Bai, Y., Ho, N., Zhao, M., Liu, Y., O'Connell, M.P., Trivedi, N.N., Nelson, C., DiMaggio, T., Jones, N., Matthews, H., Lewis, K.L., Oler, A.J., Carlson, R.J., Arkwright, P.D., Hong, C., Agama, S., Wilson, T.M., Tucker, S., Zhang, Y., McElwee, J.J., Pao, M., Glover, S.C., Rothenberg, M.E., Hohman, R.J., Stone, K.D., Caughey, G.H., Heller, T., Metcalfe, D.D., Biesecker, L.G., Schwartz, L.B., Milner, J.D., 2017. Elevated basal serum tryptase identifies a multisystem disorder associated with increased TPSAB1 copy number. Nat. Genet. 48, 1564–1569.
Maleki, M., Ghanbarvand, F., Behvarz, R.M., Ejtemaei, M., Ghadirkhomi, E., 2014. Comparison of mesenchymal stem cell markers in multiple human adult stem cells. Int J Stem Cells 7, 118–126.
Mallanna, S.K., Ormsbee, B.D., Iacovino, M., Gilmore, J.M., Cox, J.L., Kyba, M., Washburn, M.P., Rizzino, A., 2010. Proteomic analysis of Sox2-associated proteins during early stages of mouse embryonic stem cell differentiation identifies Sox21 as a novel regulator of stem cell fate. Stem Cell. 28, 1715–1727.
Marvin Jr., J.W., Chittick, L.V., Rosenthal, K.J., Sandra, A., Atkins, L.D., Hermsmeyer, K., 1984. The isolated sinoatrial node cell in primary culture from the newborn rat. Circ. Res. 55, 253–260.
McCarroll, C.S., He, W., Foote, K., Bradley, A., Mcglynn, K., Vidler, F., Nixon, C., Nather, K., Fattah, C., Riddell, A., Bowman, P., Elliott, E.B., Bell, M., Hawksby, C., MacKenzie, S.M., Morrison, L.J., Terry, A., Blyth, K., Smith, G.L., McBride, M.W., Kubin, T., Braun, T., Nicklin, S.A., Cmaeron, E.R., Loughrey, C.M., 2018. Runx1 deficiency protects against adverse cardiac remodeling after myocardial infarction. Circulation 137, 57–70.
McDaneld, T.G., Hancock, D.L., Moody, D.E., 2004. Altered mRNA abundance of ASB15 and four other genes in skeletal muscle following administration of β -adrenergic receptor agnosits. Physiol. Genom. 16, 275–283.
Morita, Y., Andersen, P., Hotta, A., Sasagawa, N., Kurokawa, J., Tsukahara, Y., Hayashida, N., Koga, C., Nishikawa, M., Evans, S.M., Furukawa, T., Koshiba-Takeuchi, K., Nishinakamura, R., Yoshida, Y., Kwon, C., Takeuchi, J.K., 2016. Sall1 transiently marks undifferentiated heart precursors and regulates their fate. J. Mol. Cell. Cardiol. 92, 158–162.
Nakayama, H., Hamatani, T., Kumagai, S., Tonegawa, K., Yamashita, T., Fujo, Y., 2018. Cardiac-specific overexpression of Runx2 mediates cardiac hypertrophy and dysfunction in mice. Circ. Res. 111, A241.
Nelms, B.L., Pfaltzgraff, E.R., Labosky, P.A., 2011. Functional interaction between foxd3 and pax3 in cardiac neural crest development. Genesis 49, 10–23.
Ortiz, M., Kaessmann, H., Zhang, K., Bashirova, A., Carrington, M., Quintana-Murci, L., Telenti, A., 2008. The evolutionary history of he CD209 (DC-SIGN) family in humans and non-human primates. Gene Immun. 9, 483–492.
Park, D.S., Fishman, G.L., 2017. Development and function of the cardiac conduction system in health and disease. J Cardiovasc Dev Dis, 2017.
Park, H.L., Bai, C., Platt, K.A., Matise, M.P., Beeghly, A., Hui, C.C., Nakashima, M., Joyner, A.L., 2000. Mouse Gli1 mutants are viable but have defects in SHH signalling in combination with a Gli2 mutation. Development 127, 1593–1605.
Petkova, M., Atkinson, J.A., Yanni, J., Stuart, L., Aminu, J.A., Ivanova, D.A., Pustovit, B.K., Geragthy, C., Feather, A., Li, N., Zhang, Y., Oceandy, D., Perde, F., Molenaar, P., D'Souza, A., Fedorov, V.V., Dobrzynski, H., 2020. Identification of key small non-coding microRNAs controlling pacemaker mechanisms in the human sinus node. J Am Heart Assoc 9, e016590.
Pinto, A.R., Godwin, J.W., Rosenthal, N.A., 2014. Macrophages in cardiac homeostasis, injury responses and progenitor cell mobilisation. Stem Cell Res. 13, 705–714.
Qin, X., Jiang, Q., Miyazaki, T., Komori, T., 2019. Runx2 regulates cranial suture closure by inducing hedgehog, Fgf, Wnt and Pthlh signaling pathway gene expressions in suture mesenchymal cells'. Hum. Mol. Genet. 28, 896–911.
Queipo-Ortuno, M.I., Escote, X., Ceperuelo-Mallafre, V., Garrido-Sanchez, L., Miranda, M., Clementee-Postigo, M., Perez-Perez, R., Peral, B., Cardona, F., Fernandez-Real, J.M., Tinahones, F.J., Vendrell, J., 2012. FABP4 dynamics in obesity: discrepancies in adipose tissue and liver expression regarding circulating plasma levels. PloS One 7, e48605.
Riddell, A., McBride, M., Braun, T., Nicklin, S.A., Cameron, E., Loughrey, C.M., Martin, T.P., 2020. Runx1: an emerging therapeutic target for cardiovas. Cardiovasc. Res. 116, 1410–1423.
Riley, P., Anson-Cartwright, L., Cross, J.C., 1998. The Hand1 bHLH transcription factor is essential for placentation and cardiac morphogenesis. Nat. Genet. 18, 271–275.
Rojo, R., Raper, A., Ozdemir, D.D., Lefevre, L., Grabert, K., Wollscheid-Lengeling, E., Bradford, B., Caruso, M., Gazova, I., Sanchez, A., Lisowski, Z.M., Alves, J., Molina-Gonzalez, I., Davtyan, H., Lodge, R.J., Glover, J.D., Wallace, R., Munro, D.A.D., David, E., Amit, I., Miron, V.E., Priller, J., Jenkins, S.J., Hardingham, G.E., Blurton-Jones, M., Mabbott, N.A., Summers, K.M., Hohensetin, P., Hume, D.A., Pridans, C., 2019. Deletion of a Csf1r enhancer selectively impacts CSF1R expression and development of tissue macrophage populations. Nat. Commun. 10, 11053–11058.
Saeed, Y., Temple, I.P., Atkinson, A., Yanni, J., Maczewski, M., Aly, M., Logantha, S.J.R.J., Garratt, C.J., Dobrzynski, H., 2018. Structural and functional remodeling of the atrioventricular node with aging in rate: the role of hyperpolarization-activated cyclic nucleotide-gated and ryanodine 2 channels. Heart Rhythm 15, 752–760.
Schweizer, A.P., Darche, F.F., Ullrich, D.N., Geschwill, P., Greber, B., Rivinius, R., Seyler, C., Muller, D.K., Draguhn, A., Utikal, J., Koenen, M., Katus, A.H., Thomas, D., 2017. Subtype-specific differentiation of cardiac pacemaker cell clusters from human induced pluripotent stem cells. Stem Cell Res. Ther. 8, 229.
Shiraishi, I., Takamatsu, T., Minamikawa, T., Onouchi, Z., Fujita, S., 1992. Quantitative histological analysis of the human sinoatrial node during growth and aging. Circulation 85, 176–184.
Starzyk, R.M., Rosenow, C., Frye, J., Leismann, M., Rodzinski, E., Putney, S., Tuomanen, E.I., 2000. Cerebral cell adhesion molecule: a novel leukocyte adhesion determinant on blood-brain barrier capillary endothelium. J. Infect. Dis. 181, 181–187.
Stephenson, S.R., Atkinson, A., Kottas, P., Perde, F., Jafarzadeh, F., Bateman, M., Iaizzo, A.P., Zhao, J., Zhang, H., Anderson, H.R., Jarvis, C.J., Dobrzynski, H., 2017. High resolution 3-dimensional imaging of the human cardiac conduction system from microanatomy to mathematical modeling. Sci. Rep. 7, 1–13.
Stephenson, S.R., Boyett, R.M., Hart, G., Nikolaidou, T., Cai, Xue, Corno, F.A., Alphonso, N., Jeffery, N., Jarvis, C.J., 2012. Contrast enhanced micro-computed tomography resolves the 3-dimensional morphology of the cardiac conduction system in mammalian hearts. PloS One 7, e35299.
Sunwoo, J.B., Kim, S., Yang, L., Naik, T., Higuchi, A.D., Rubenstein, L.J., Yokoyama, W.M., 2008. Distal-less homeobox transcription factors regulate development and maturation of natural killer cells. Proc. Natl. Acad. Sci. Unit. States Am. 105, 10877–10882.
Swirski, K.F., Nahendorf, M., 2018. Cardioimmunology: the immune system in cardiac homeostasis and disease. Nat. Rev. Immunol. 18, 733–744.
Tang, H., Gao, Y., Li, Z., Miao, Y., Huang, Z., Liu, X., Xie, L., Wen, W., Zheng, Y., Su, W., 2020. The noncoding and coding transcriptional landscape of the peripheral immune response in patients with COVID-19. Clin. Transl. Med. 10, e200.
Tessadori, F., van Weerd, H.J., Burkhard, B.S., Verkerk, O.A., de Pater, E., Boukens, J.B., Vink, A., Christoffels, M.V., Bakkers, J., 2012. Identification and functional characterization of cardiac pacemaker cells in zebrafish. PloS One 7, e47644.
Thum, T., Galuppo, P., Wolf, C., Fiedler, J., Kneitz, S., van Laake, L.W., Doevendans, A.P., Mummery, C.L., Borlak, J., Haverich, A., Gross, C., Engelhardt, S., Ertl, G., Bauersach, J., 2007. MicroRNAs in the human heart: a clue to fetal gene reprogramming in heart failure. Circulation 17, 258–267.
van der Deen, M., Akech, J., Lapointe, D., Gupta, S., Young, W.D., Montecino, A.M., Galindo, M., Lian, B.J., Stein, L.J., Stein, S.G., van Wijnen, J.A., 2012. Genomic promoter occupancy of runt-related transcription factor RUNX2 in osteosarcoma cells identifies genes involved in cell adhesion and motility. J. Biol. Chem. 287, 4503–4517.
van Eif, V.W.W., Stefanovic, S., van Duijvenboden, K., Bakker, M., Wakker, V., de Gier-de Vries, C., Zaffran, S., Verkerk, A.O., Boukens, B.J., Christoffels, V.M., 2019. Transcriptome analysis of mouse and human sinoatrial node cells reveals a conserved genetic program. Development 146, dev173161.
van Eif, W.W.V., Devalla, D.H., Boink, J.J.G., Christoffels, M.V., 2018. Transcriptional regulation of the cardiac conduction system. Nat. Rev. Cardiol. 15, 1–14.

Vasconcelos, F.F., Sessa, A., Laranjeira, C., Raposo, A.A.S.F., Teixeira, V., Hagey, D.W., Tomaz, D.M., Muhr, J., Broccoli, V., Castro, D.S., 2016. MyT1 counteracts the neural progenitor program to promote vertebrate neurogenesis. Cell Rep. 17, 469–483.

Wangler, M.F., Gonzaga-Jauregui, C., Gambin, T., Penney, S., Moss, T., Chopra, A., Probst, F.J., Xia, F., Yang, Y., Werlin, S., Eglite, I., Kornejeva, L., Bacino, A.C., Baldridge, D., Neul, J., Lehman, E.L., Larson, A., Beuten, J., Muzny, D.M., Jhangiani, S., B-HCMG, Gibbs, R.A., Lupski, J.R., Beaudet, A., 2014. Heterodygous de novo and inherited mutations in the smooth muscle actin (ACTG2) gene underlie megacystis-mircocolon-interstinal hypoperistalsis syndrome. PLoS Genet. 10, e1004258.

Williams, M.W., Bloch, R.J., 1999. Differential distribution of dystrophin and beta-spectrin at the sarcolemma of fast twitch skeletal muscle fibres. J. Muscle Res. Cell Motil. 20, 383–393.

Wong, H.H., Seet, S.H., Bascom, C.C., Isfort, R.J., Bard, F., 2020. Red-COLA1: a human fibroblast reporter cell line for type I collagen transcription. Sci. Rep. 10, 1–12.

Wynn, T.A., 2009. Cellular and molecular mechanisms of fibrosis. J. Pathol. 214, 199–210.

Xiao, Q., Hou, N., Wang, Y.-P., Zhang, G.-P., Yi, Q., Liu, S.-M., Chen, M.-S., Luo, J.-D., 2012. Impaired sonic hedgehog pathway contributes to cardiac dysfunction in type 1 diabetic mice with myocardial infarction. Cardiovasc. Res. 95, 507–516.

Yamamoto, M., Abe, S.-I., Rodriguez-Vazquez, J.F., Fajimiya, M., Murakami, G., Ide, Y., 2011. Immunohistochemical distribution of desmin in the human fetal heart. J. Anat. 219, 253–258.

Zanetti, M., Braghetta, P., Sabatelli, P., Mura, I., Doliana, R., Colombatti, A., Volpin, D., Bonaldo, P., Bressan, G.M., 2004. EMILIN-1 deficiency induces elastogenesis and vascular cell defects. Mol. Cell Biol. 24, 638–650.

Zhang, H., Holden, A.V., Kodama, I., Honjo, M., Lei, M., Varghese, T., Boyett, R.M., 2000. Mathematical models of action potentials in the periphery and center of the rabbit sinoatrial node. Am. J. Physiol. 279, 397–421.

Zhang, H., Tian, L., Shen, M., Tu, C., Wu, H., Gu, M., Paik, D.T., Wu, J.C., 2019. Generation of quiescent cardiac fibroblasts from human induced pluripotent stem cells for in vitro modeling of cardiac fibrosis. Circ. Res. 125, 552–566.

Zicha, S., Fernandez-Velasco, M., Lonardo, G., L'Heureux, N., Nattel, S., 2005. Sinus node dysfunction and hyperpolarization-activated (HCN) channel subunit remodelling in a canine heart failure model. Cardiovasc. Res. 66, 472–481.

Zriwil, A., Boiers, C., Wittmann, L., Green, J.C.A., Woll, P.S., Jacobsen, S.E.W., Sitnicka, E., 2016. Macrophage colony-stimulating factor receptor marks and regulates a fetal myeloid-primed B-cell progenitor in mice. Blood 128, 217–226.